# Efficient High Order Waveguide Mode Solvers based on Boundary Integral Equations[☆]

Wangtao Lu[a,b], Ya Yan Lu[a]

[a]*Department of Mathematics, City University of Hong Kong, Kowloon, Hong Kong*
[b]*Department of Mathematics, Michigan State University, East Lansing, MI 48824, USA*

---

## Abstract

For optical waveguides with high index contrast and sharp corners, high order full-vectorial mode solvers are difficult to develop, due to the field singularities at the corners. A recently developed method (the so-called BIE-NtD method) based on boundary integral equations (BIEs) and Neumann-to-Dirichlet (NtD) maps achieves high order of accuracy for dielectric waveguides. In this paper, we develop two new BIE mode solvers, including an improved version of the BIE-NtD method and a new BIE-DtN method based on Dirichlet-to-Neumann (DtN) maps. For homogeneous domains with sharp corners, we propose better BIEs to compute the DtN and NtD maps, and new kernel-splitting techniques to discretize hypersingular operators. Numerical results indicate that the new methods are more efficient and more accurate, and work very well for metallic waveguides and waveguides with extended mode profiles.

*Keywords:* Optical waveguides, boundary integral equations,
Dirichlet-to-Neumann map, Neumann-to-Dirichlet map, mode solvers,
hypersingular integral operators

---

## 1. Introduction

Optical waveguides [1, 2, 3] are structures that can guide the propagation of light. They are widely used as basic components in integrated optical

---

*Email addresses:* `wangtaol@math.msu.edu` (Wangtao Lu), `mayylu@cityu.edu.hk` (Ya Yan Lu)

circuits and optical communication systems. In recent years, many complicated optical waveguides have appeared, such as photonic crystal fibers [4], plasmonic waveguides [5], etc. These new waveguides have attracted much attention due to their unique abilities in confining light. For an optical waveguide, the most important mathematical problem is the computation of waveguide modes. For a waveguide which is invariant along its axis $z$, a guided mode is a special solution of Maxwell's equations that depends on $z$ as $\exp(i\beta z)$ and decays exponentially away from the waveguide core, where $\beta$ is the so-called propagation constant. Open waveguides also have leaky modes which exhibit outgoing wave behavior away from the waveguide core. Throughout this paper, we consider only guided modes.

Classical optical fibers can be studied using a scalar model, since the refractive indices of the core and the cladding are nearly equal. There are also semi-vectorial models that are applicable to some waveguides. For waveguides with high index contrast, such as silicon waveguides, plasmonic waveguides and photonic crystal fibers, full-vectorial methods are necessary. Currently, there exist many different full-vectorial mode solvers, including the finite difference method [6, 7, 8, 9, 10, 11, 12, 13, 14], the finite element method [15, 16, 17, 18, 19, 20, 21, 22], the multi-domain pseudospectral method [23, 24, 25], etc. However, for waveguides with sharp corners, it is very difficult to find any high order numerical method, since the electromagnetic field may be singular at the corners.

Boundary integral equation (BIE) methods have been used to analyze optical waveguides [26, 27, 28, 29, 30, 31, 33, 32]. They are highly competitive, since they can easily handle general refractive-index discontinuities (i.e., interfaces), discretize on the interfaces only, and give rise to small matrices. Existing BIE methods reported in [26, 27, 28] exhibit low convergence orders due to their use of boundary elements. For waveguides with smooth interfaces, high order BIE methods with exponential convergence are available [29, 30, 31]. However, these high order methods need to solve four functions on each interface. In a recent work [32], we developed a high order BIE method that solves only two functions on each interface. Our method also has exponential convergence, and is almost eight times faster than other BIE methods. We call this method BIE-DtN method, since it relies on the Dirichlet-to-Neumann (DtN) map for each homogeneous domain (with a constant refractive index). However, all these high-order BIE methods encounter difficulties when the waveguide has sharp corners, since the methods used in these papers for discretizing boundary integral operators could fail. In [33],

we developed a high order full-vectorial BIE mode solver for waveguides with sharp corners. We call this method the BIE-NtD method, since it relies on the Neuman-to-Dirichlet (NtD) map for each homogeneous domain. The method achieves high order convergence for dielectric waveguides with corners, but it needs to solve four functions on each interface.

In this paper, we develop new versions for both BIE-DtN and BIE-NtD methods. The new BIE-DtN method still solves two functions on each interface, but now handles waveguides with sharp corners. The DtN map for a general domain with corners is computed using a BIE with a hypersingular integral operator and extra terms corresponding to the corners. For the hypersingular integral operator on a smooth boundary, Kress [34] developed a high-order kernel-splitting technique for its discretization, but the method fails on boundaries with corners. We develop a new kernel-splitting technique to overcome this difficulty. Our new BIE-NtD method still handles waveguides with sharp corners, but solves three (instead of four) functions on each interface. Although it still solves one more function than the BIE-DtN method, the BIE-NtD method is simpler to implement. Furthermore, many optical waveguides have interfaces extending to infinity, leading to domains of constant refractive index with unbounded boundaries. We also develop well-approximated BIEs to compute both DtN and NtD maps for these domains. Overall, these new BIE mode solvers are more general and solve minimum number of unknowns on each interface. As illustrated by the numerical examples, these new methods bring a large saving in the computational cost and a significant improvement in the accuracy.

## 2. Problem formulations

To illustrate the basic ideas clearly, we start with a simple case where the optical waveguide involves a finite core surrounded by a homogeneous medium (the cladding) as shown in Fig. 1. The waveguide structure is invariant in the $z$-direction, and its cross-section in the $xy$-plane consists of two homogeneous domains, a bounded domain $\Omega_1$ with refractive index $n_1$ and an unbounded domain $\Omega_2$ with refractive index $n_2$, which share a common boundary $\Gamma$. Both the core and the cladding are assumed to be non-magnetic. For dielectric waveguides, the refractive indices satisfy $n_1 > n_2$. We also consider metallic waveguides for which $n_1$ is complex. Here $\{x, y, z\}$ is the standard Cartesian coordinate system. In the following, we only consider homogeneous domains with Lipschitz and piecewise smooth boundaries. For
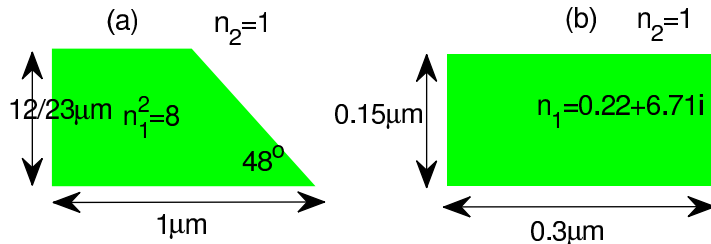
Figure 1: Waveguides with a single core surrounded by a homogeneous medium: (a) a dielectric waveguide with a trapezoidal core; (b) a metallic waveguide with a rectangular core.

time harmonic waves with the time dependence $\exp(-i\omega t)$ where $\omega$ is the angular frequency, the governing Maxwell's equations are

$$\nabla \times \boldsymbol{E} = ik_0\boldsymbol{H}, \tag{1}$$
$$\nabla \times \boldsymbol{H} = -ik_0\varepsilon\boldsymbol{E}. \tag{2}$$

In the above, $\nabla$ denotes the gradient operator, $\boldsymbol{E}$ is the electric field, $\boldsymbol{H}$ is the magnetic field multiplied by the freespace impedance, $k_0 = \omega/c = 2\pi/\lambda$ is the freespace wavenumber, $c$ is the speed of light in vacuum, $\lambda$ is the free space wavelength, $\varepsilon = n^2$ is the dielectric function, and it is piecewise constant and independent of $z$. On the interface $\Gamma$, the four components $E_z$, $H_z$, $H_x$ and $H_y$ are continuous where $E_z$ denotes the $z$-component of $\boldsymbol{E}$, etc.

A guided mode of the waveguide is a special solution of Eqs. (1) and (2) such that both $\boldsymbol{E}$ and $\boldsymbol{H}$ depend on $z$ as $\exp(i\beta z)$ and decay exponentially to zero as $\sqrt{x^2 + y^2} \to \infty$, where $\beta$ is called the propagation constant. To find $\beta$, BIE methods typically work on only two components: $\{E_z, H_z\}$ or $\{H_x, H_y\}$. For waveguides with non-magnetic media and domains with corners, we prefer to use $\{H_x, H_y\}$, since they are smoother than other components, and finite even at corners. In each domain $\Omega_j$, both $H_x$ and $H_y$ satisfy the following Helmholtz equation

$$\partial_x^2 u + \partial_y^2 u + \gamma_j^2 u = 0, \tag{3}$$

where $\gamma_j^2 = k_0^2\varepsilon_j - \beta^2$ and $\varepsilon_j = n_j^2$ for $j = 1, 2$. On the interface $\Gamma$, $H_x$ and $H_y$ themselves are continuous. From Maxwell's equations, the continuities of $E_z$ and $H_z$ imply that

$$\partial_x H_x + \partial_y H_y \quad \text{and} \quad \frac{1}{\varepsilon}(\partial_x H_y - \partial_y H_x) \tag{4}$$

4

are also continuous. Writing (4) as linear combinations of the tangential and normal derivatives of $H_x$ and $H_y$, it is easy to see that

$$\nu_x \partial_{\boldsymbol{\nu}} H_x + \nu_y \partial_{\boldsymbol{\nu}} H_y \text{ and } \frac{1}{\varepsilon} \left[ (\nu_x \partial_{\boldsymbol{\nu}} H_y - \nu_y \partial_{\boldsymbol{\nu}} H_x) - (\nu_y \partial_{\boldsymbol{\tau}} H_y + \nu_x \partial_{\boldsymbol{\tau}} H_x) \right] \quad (5)$$

are continuous across $\Gamma$, where $\boldsymbol{\nu} = (\nu_x, \nu_y)$ denotes the unit normal vector of $\Gamma$ pointing to the exterior domain $\Omega_2$, and $\boldsymbol{\tau} = (-\nu_y, \nu_x)$ denotes the unit tangential vector along $\Gamma$.

Existing waveguide mode solvers based on BIE formulations can be classified as indirect methods (see [29, 30, 31]) and direct methods (see [26, 27, 28, 32, 33]). In an indirect method, each of the two components (such as $H_x$ and $H_y$) is written as layer potentials with two (exterior and interior) density functions defined on the interface $\Gamma$. These methods are not so convenient for computing tangential derivatives and need to solve four functions on $\Gamma$. We prefer to use direct methods, since they are more convenient for computing the tangential derivatives and may lead to less functions on $\Gamma$.

Before presenting the direct BIE formulations, we define some operators for each homogeneous domain $\Omega_j$ and the corresponding Helmholtz equation (3). The DtN operator $\Lambda_j$ maps $u$ to $\partial_{\boldsymbol{\nu}} u$, i.e., $\Lambda_j u = \partial_{\boldsymbol{\nu}} u$, on $\Gamma$ for all $u$ satisfying Eq. (3). The NtD operator $\mathcal{N}_j$ maps $\partial_{\boldsymbol{\nu}} u$ to $u$, i.e., $\mathcal{N}_j \partial_{\boldsymbol{\nu}} u = u$, on $\Gamma$ for all $u$ satisfying Eq. (3). Clearly, $\mathcal{N}_j$ is the inverse of $\Lambda_j$, and both are related to $\beta$. In the following, we also need the tangential derivative operator $\partial_{\boldsymbol{\tau}}$ on $\Gamma$.

In [32], we developed a two-function BIE-DtN formulation for waveguides with smooth interfaces. When $\Gamma$ has corners, the formulation can still be used provided that both $\Lambda_1$ and $\Lambda_2$ are calculated accurately. More specifically, from (5), we have

$$\begin{bmatrix} \nu_x \Lambda_2 - \nu_x \Lambda_1 & \nu_y \Lambda_2 - \nu_y \Lambda_1 \\ \rho \nu_x \partial_{\boldsymbol{\tau}} + \nu_y \Pi & \rho \nu_y \partial_{\boldsymbol{\tau}} - \nu_x \Pi \end{bmatrix} \begin{bmatrix} H_x \\ H_y \end{bmatrix} = 0 \quad \text{on} \quad \Gamma, \quad (6)$$

where

$$\Pi = \varepsilon_1^{-1} \Lambda_1 - \varepsilon_2^{-1} \Lambda_2, \quad \rho = \varepsilon_1^{-1} - \varepsilon_2^{-1}. \quad (7)$$

The matrix operator in the left hand side of (6) depends non-linearly on $\beta$. Once $\partial_{\boldsymbol{\tau}}$ and $\Lambda_j$ are approximated, we can find $\beta$ numerically. As mentioned before, the key step of this formulation is to compute the DtN operators for

domains with corners. The details of this step will be presented in the next section.

The BIE-NtD method developed in [33] uses a four-function formulation. On the interface $\Gamma$, the method makes use of the continuities of $H_x$, $H_y$ and the two terms in (4). Writing all of them in terms of $\partial_\nu H_x^+$, $\partial_\nu H_y^+$, $\partial_\nu H_x^-$ and $\partial_\nu H_y^-$ (where the superscripts $'+'$ and $'-'$ indicate limits taken from the exterior domain $\Omega_2$ and the interior domain $\Omega_1$, respectively), the following nonlinear eigenvalue problem on $\Gamma$ is established:

$$
\begin{bmatrix}
\mathcal{A}_2 & \mathcal{B}_2 & -\mathcal{A}_1 & -\mathcal{B}_1 \\
-\varepsilon_2^{-1}\mathcal{B}_2 & \varepsilon_2^{-1}\mathcal{A}_2 & \varepsilon_1^{-1}\mathcal{B}_1 & -\varepsilon_1^{-1}\mathcal{A}_1 \\
\mathcal{N}_2 & 0 & -\mathcal{N}_1 & 0 \\
0 & \mathcal{N}_2 & 0 & -\mathcal{N}_1
\end{bmatrix}
\begin{bmatrix}
\partial_\nu H_x^+ \\
\partial_\nu H_y^+ \\
\partial_\nu H_x^- \\
\partial_\nu H_y^-
\end{bmatrix} = 0. \tag{8}
$$

In the above, the tangential derivative operator $\partial_\tau$ and the NtD operators $\mathcal{N}_2$ and $\mathcal{N}_1$ are needed, and

$$
\mathcal{A}_j = \nu_x - \nu_y \partial_\tau \circ \mathcal{N}_j, \quad \mathcal{B}_j = \nu_y + \nu_x \partial_\tau \circ \mathcal{N}_j \tag{9}
$$

for $j = 1, 2$.

It is possible to reduce the number of required functions for the BIE-NtD approach. In fact, from (5), we can see that

$$
\nu_x \partial_\nu H_x^+ + \nu_y \partial_\nu H_y^+ = \nu_x \partial_\nu H_x^- + \nu_y \partial_\nu H_y^-. \tag{10}
$$

This allows us to establish a new nonlinear eigenvalue problem involving three functions only. More precisely, let $f = \nu_x \partial_\nu H_x^\pm + \nu_y \partial_\nu H_y^\pm$ and $g^\pm = -\nu_y \partial_\nu H_x^\pm + \nu_x \partial_\nu H_y^\pm$, then the continuities of $H_x$, $H_y$ and the two terms in (5) give rise to

$$
\begin{bmatrix}
\varepsilon_1^{-1}\mathcal{F}_1 - \varepsilon_2^{-1}\mathcal{F}_2 & \varepsilon_2^{-1}\mathcal{E}_2 & -\varepsilon_1^{-1}\mathcal{E}_1 \\
(\mathcal{N}_2 - \mathcal{N}_1)(\nu_x \cdot) & -\mathcal{N}_2(\nu_y \cdot) & \mathcal{N}_1(\nu_y \cdot) \\
(\mathcal{N}_2 - \mathcal{N}_1)(\nu_x \cdot) & \mathcal{N}_2(\nu_x \cdot) & -\mathcal{N}_1(\nu_x \cdot)
\end{bmatrix}
\begin{bmatrix}
f \\
g^+ \\
g^-
\end{bmatrix} = 0, \tag{11}
$$

where
$$
\mathcal{E}_j = \mathcal{A}_j(\nu_x \cdot) + \mathcal{B}_j(\nu_y \cdot), \quad \mathcal{F}_j = -\mathcal{A}_j(\nu_y \cdot) + \mathcal{B}_j(\nu_x \cdot), \tag{12}
$$

for $j = 1, 2$ and $\mathcal{N}_1(\nu_x \cdot)f = \mathcal{N}_1(\nu_x f)$, etc. Therefore, we can find $\beta$ after $\partial_\tau$ and $\mathcal{N}_j$ are approximated. Compared with Eq. (8), the new three-function BIE-NtD formulation reduces the matrix size by 25%.

## 3. DtN and NtD operators

In this section, we present the BIEs for computing the DtN and NtD operators. The fundamental solution of Eq. (3) is

$$G^{(j)}(\boldsymbol{r}, \tilde{\boldsymbol{r}}) = \frac{i}{4} H_0^{(1)}(\gamma_j |\boldsymbol{r} - \tilde{\boldsymbol{r}}|), \quad \boldsymbol{r} \neq \tilde{\boldsymbol{r}}, \tag{13}$$

for $j = 1, 2$, where $\boldsymbol{r} = (x, y)$, $\tilde{\boldsymbol{r}} = (\tilde{x}, \tilde{y})$, and $H_0^{(1)}$ is the first-kind Hankel function of zeroth order. The BIEs involve the following four boundary integral operators:

$$(\mathcal{S}_j \phi)(\boldsymbol{r}) = 2 \int_\Gamma G^{(j)}(\boldsymbol{r}, \tilde{\boldsymbol{r}}) \phi(\tilde{\boldsymbol{r}}) ds(\tilde{\boldsymbol{r}}), \quad \boldsymbol{r} \in \Gamma, \tag{14}$$

$$(\mathcal{K}_j \phi)(\boldsymbol{r}) = 2 \fint_\Gamma \frac{\partial G^{(j)}(\boldsymbol{r}, \tilde{\boldsymbol{r}})}{\partial \boldsymbol{\nu}(\tilde{\boldsymbol{r}})} \phi(\tilde{\boldsymbol{r}}) ds(\tilde{\boldsymbol{r}}), \quad \boldsymbol{r} \in \Gamma, \tag{15}$$

$$(\mathcal{K}_j' \phi)(\boldsymbol{r}) = 2 \fint_\Gamma \frac{\partial G^{(j)}(\boldsymbol{r}, \tilde{\boldsymbol{r}})}{\partial \boldsymbol{\nu}(\boldsymbol{r})} \phi(\tilde{\boldsymbol{r}}) ds(\tilde{\boldsymbol{r}}), \quad \boldsymbol{r} \in \Gamma, \tag{16}$$

$$(\mathcal{T}_j \phi)(\boldsymbol{r}) = 2 \ffint_\Gamma \frac{\partial^2 G^{(j)}(\boldsymbol{r}, \tilde{\boldsymbol{r}})}{\partial \boldsymbol{\nu}(\boldsymbol{r}) \partial \boldsymbol{\nu}(\tilde{\boldsymbol{r}})} \phi(\tilde{\boldsymbol{r}}) ds(\tilde{\boldsymbol{r}}), \quad \boldsymbol{r} \in \Gamma, \tag{17}$$

where $\fint$ denotes the Cauchy principle value integral and $\ffint$ denotes the Hadamard finite part integral.

Consider the bounded domain $\Omega_1$ first. If $\Gamma$ is smooth and $u \in C^\infty(\overline{\Omega}_1)$, we have the following boundary integral equations

$$(1 + \mathcal{K}_1)u = \mathcal{S}_1 \partial_{\boldsymbol{\nu}} u, \quad \text{on} \quad \Gamma, \tag{18}$$

$$(\mathcal{K}_1' - 1)\partial_{\boldsymbol{\nu}} u = \mathcal{T}_1 u, \quad \text{on} \quad \Gamma. \tag{19}$$

Note that this regularity assumption on $u$ can be weakened (see [35]). Therefore, if $\gamma_1^2$ is not an eigenvalue of the associated homogeneous Dirichlet or Neumann problem of Eq. (3), then the NtD and DtN operators are given by

$$\mathcal{N}_1 = (1 + \mathcal{K}_1)^{-1} \mathcal{S}_1, \quad \Lambda_1 = (\mathcal{K}_1' - 1)^{-1} \mathcal{T}_1. \tag{20}$$

For the more general case where $\Gamma$ is piecewise smooth and has corners, Eqs. (18) and (19) are not valid at the corners. The modified BIE related to the NtD operator is

$$(\mathcal{K}_1 - \mathcal{K}_0 1)u = \mathcal{S}_1 \partial_{\boldsymbol{\nu}} u, \quad \text{on} \quad \Gamma, \tag{21}$$

where $\mathcal{K}_0$ is the operator defined by

$$(\mathcal{K}_0\phi)(\boldsymbol{r}) = 2\fint_\Gamma \frac{\partial G_0(\boldsymbol{r},\tilde{\boldsymbol{r}})}{\partial \boldsymbol{\nu}(\tilde{\boldsymbol{r}})}\phi(\tilde{\boldsymbol{r}})ds(\tilde{\boldsymbol{r}}), \quad \boldsymbol{r} \in \Gamma, \tag{22}$$

and $G_0$ is the Green's function of Laplace equation, that is

$$G_0(\boldsymbol{r},\tilde{\boldsymbol{r}}) = -\frac{1}{2\pi}\log|\boldsymbol{r}-\tilde{\boldsymbol{r}}|, \quad \boldsymbol{r} \neq \tilde{\boldsymbol{r}}.$$

Therefore, the NtD operator is given by

$$\mathcal{N}_1 = (\mathcal{K}_1 - \mathcal{K}_0 1)^{-1}\mathcal{S}_1. \tag{23}$$

Eq. (21) has been used in [33] for computing the NtD operators for domains with corners. A very weak sufficient condition on $u$ and a rigorous derivation of this BIE is given in Appendix. Notice that

$$(\mathcal{K}_0 1)(\boldsymbol{r}) = -\frac{\theta(\boldsymbol{r})}{\pi},$$

where $\theta(\boldsymbol{r})$ is the interior angle of $\Omega$ at $\boldsymbol{r} \in \Gamma$. Thus, Eq. (21) is the same as

$$\left(\mathcal{K}_1 + \frac{\theta}{\pi}\right)u = \mathcal{S}\partial_{\boldsymbol{\nu}}u, \quad \text{on} \quad \Gamma.$$

Although $\mathcal{K}_0 1$ is known explicitly, we prefer to use Eq. (21) and evaluate it numerically. The reason is that when $\boldsymbol{r}$ is extremely close to a corner point, the discretization of the improper integral $(\mathcal{K}_1 u)(\boldsymbol{r})$ has numerical errors which appear to be cancelled out to some extent through a consistent numerical evaluation of $\mathcal{K}_0 1$. We present numerical evidences for this claim in section 6.

The BIE (19) related to the DtN operator remains valid only for smooth points of $\Gamma$, i.e.,

$$(\mathcal{K}_1'\partial_{\boldsymbol{\nu}}u)(\boldsymbol{r}) - \partial_{\boldsymbol{\nu}}u(\boldsymbol{r}) = (\mathcal{T}_1 u)(\boldsymbol{r}), \tag{24}$$

where $\boldsymbol{r}$ can be any smooth point of $\Gamma$. Once again, significant numerical errors appear when $\boldsymbol{r}$ is extremely close to a corner point when the two improper integrals in (24) are discretized. Our approach is to use the following BIE

$$(\mathcal{K}_1'\partial_{\boldsymbol{\nu}}u)(\boldsymbol{r}) + (\mathcal{K}_0 1)(\boldsymbol{r})\partial_{\boldsymbol{\nu}}u(\boldsymbol{r}) = (\mathcal{S}_0'1)(\boldsymbol{r})\partial_{\boldsymbol{\tau}}u(\boldsymbol{r}) + (\mathcal{T}_1 u)(\boldsymbol{r}), \tag{25}$$

where $\boldsymbol{r}$ is any smooth point on $\Gamma$ and

$$(\mathcal{S}_0'\phi)(\boldsymbol{r}) = 2\fint_\Gamma \frac{\partial G_0(\boldsymbol{r},\tilde{\boldsymbol{r}})}{\partial\boldsymbol{\tau}(\tilde{\boldsymbol{r}})}\phi(\tilde{\boldsymbol{r}})ds(\tilde{\boldsymbol{r}}). \tag{26}$$

A very weak sufficient regularity condition on $u$ and a derivation of Eq. (25) are presented in Appendix. Therefore, the DtN operator can be calculated by

$$\Lambda_1 = (\mathcal{K}_1' + \mathcal{K}_0 1)^{-1}(\mathcal{S}_0'1\partial_\tau + \mathcal{T}_1). \tag{27}$$

Actually, it is easy to verify that $(\mathcal{S}_0'1)(\boldsymbol{r}) = 0$ and $(\mathcal{K}_0 1)(\boldsymbol{r}) = -1$ on the smooth part of $\Gamma$, thus the two BIEs (24) and (25) are exactly the same away from the corner points. As before, $\mathcal{K}_0 1$ and $\mathcal{S}_0'1$ are evaluated numerically together with the other integral operators. Numerical evidences for their usefulness are presented in section 6.

For the unbounded domain $\Omega_2$, each field component of the guided mode decays exponentially to 0 as $r = \sqrt{x^2 + y^2} \to \infty$. If $R > 0$ is large enough so that the open disk $B_O(R) = \{(x,y)|x^2 + y^2 < R^2\}$ contains $\Omega_1$, we can establish BIEs like (21) and (25) for the truncated domain $\Omega_2 \cap B_O(R)$. As $R \to \infty$, we obtain

$$(\mathcal{K}_2 - \mathcal{K}_0 1 - 2)u = \mathcal{S}_2\partial_\nu u, \quad \text{on} \quad \Gamma, \tag{28}$$

$$(\mathcal{K}_0 1 + \mathcal{K}_2' + 2)\partial_\nu u = \mathcal{S}_0'1\partial_\tau u + \mathcal{T}_2 u, \quad \text{on smooth points of } \Gamma. \tag{29}$$

Therefore, the NtD and DtN operators for $\Omega_2$ are given by

$$\mathcal{N}_2 = (\mathcal{K}_2 - \mathcal{K}_0 1 - 2)^{-1}\mathcal{S}_2, \tag{30}$$

$$\Lambda_2 = (\mathcal{K}_2 - \mathcal{K}_0 1 - 2)^{-1}(\mathcal{S}_0'1\partial_\tau + \mathcal{T}_2). \tag{31}$$

To approximate $\mathcal{N}_j$ and $\Lambda_j$, we need to approximate the involved integral operators first. We present the details in the following sections. Since $u$ represents $H_x$ or $H_y$, in the rest of this paper (except for Appendix), we will assume $u$ and $\partial_\nu u$ are smooth at smooth points on $\Gamma$ and $u$ is continuous at the corners [9, 10, 27, 28]. Note that the one-sided limits of $\partial_\nu u$ and $\partial_\tau u$ may diverge at the corners.

## 4. Kernel-splitting technique: smooth case

In this section, we briefly review the Nyström method with kernel-splitting techniques for the case when $\Gamma$ is smooth, and introduce a new stabilized splitting technique to prevent numerical instability for metallic waveguides.

Without loss of generality, we consider the bounded domain $\Omega_1$ and assume $\Gamma$ is given by

$$\boldsymbol{r}(\eta) = (x(\eta), y(\eta)), \quad 0 \leq \eta \leq 2\pi,$$

where both $x(\eta)$ and $y(\eta)$ are analytic functions and $|\boldsymbol{r}'(\eta)| > 0$ for all $\eta$. We need to discretize $\mathcal{S}_1$, $\mathcal{K}_1$, $\mathcal{K}_1'$ and $\mathcal{T}_1$. For the first three operators, since all of them are weakly singular, following [35, 34], we can transform each of $\mathcal{S}_1$, $\mathcal{K}_1$ and $|\boldsymbol{r}'|\mathcal{K}_1'$ (not $\mathcal{K}_1'$) to the following general form

$$\int_0^{2\pi} h(\eta, \tilde{\eta})\phi(\tilde{\eta})d\tilde{\eta}, \tag{32}$$

where $\phi$ corresponds to a $2\pi$-periodic smooth function. The kernel $h$ can be splitted as the sum of a smooth part and a part with a simple logarithmic singularity, i.e.,

$$h(\eta, \tilde{\eta}) = h_1(\eta, \tilde{\eta}) \log \left(4 \sin^2 \frac{\eta - \tilde{\eta}}{2}\right) + h_2(\eta, \tilde{\eta}),$$

where both $h_1$ and $h_2$ are analytic. If $\eta$ is uniformly discretized by $N$ points $\{\eta_l = l\pi/N\}_{l=0}^{N-1}$ where $N$ is even, the integral of $h_2$ can be approximated by the trapezoidal rule. The integral of the logarithmic term can be approximated by the following quadrature formula of Martensen and Kussmaul [37]:

$$\int_0^{2\pi} \phi(\tilde{\eta}) \log \left(4 \sin^2 \frac{\eta - \tilde{\eta}}{2}\right) d\tilde{\eta} \approx \sum_{l=0}^{N-1} R_l^N(\eta)\phi(\eta_l), \tag{33}$$

where

$$R_l^N(\eta) = -\frac{4\pi}{N} \sum_{k=0}^{N/2-1} \frac{1}{k} \cos[k(\eta - \eta_l)] - \frac{4\pi}{N^2} \cos[N(\eta - \eta_l)/2].$$

Therefore, (32) is approximated by

$$\sum_{l=0}^{N-1} \left[ R_l^N(\eta)h_1(\eta, \eta_l) + \frac{2\pi}{N} h_2(\eta, \eta_l) \right] \phi(\eta_l).$$

For more details, we refer readers to [35, 34].

The kernel-splitting technique for the hypersingular operator $\mathcal{T}_1$ was developed by Kress [34]. First, we make use of Maue's identity (multiplied by $|\boldsymbol{r}'|$),

$$|\boldsymbol{r}'|\mathcal{T}_1 u = |\boldsymbol{r}'|\mathcal{S}_1'\partial_{\boldsymbol{\tau}} u + \gamma_1^2 |\boldsymbol{r}'|\boldsymbol{\nu} \cdot \mathcal{S}_1(\boldsymbol{\nu} u), \tag{34}$$

10

where

$$(\mathcal{S}_1' \partial_\tau u)(\boldsymbol{r}) = 2 \fint_\Gamma \frac{\partial G^{(1)}(\boldsymbol{r}, \tilde{\boldsymbol{r}})}{\partial \boldsymbol{\tau}(\boldsymbol{r})} \partial_\tau u(\tilde{\boldsymbol{r}}) ds(\tilde{\boldsymbol{r}}), \quad \boldsymbol{r} \in \Gamma. \tag{35}$$

The key step is to approximate $\mathcal{S}_1' \partial_\tau u$ since the second term in the right side of (34) only involves the operator $\mathcal{S}_1$. By splitting out a singular term and integration by parts, we can transform $|\boldsymbol{r}'|\mathcal{S}_1' \partial_\tau u$ to

$$\frac{1}{2\pi} \int_0^{2\pi} \cot \frac{\tilde{\eta} - \eta}{2} \frac{du(\boldsymbol{r}(\tilde{\eta}))}{d\tilde{\eta}} d\tilde{\eta} - \int_0^{2\pi} M(\eta, \tilde{\eta}) u(\boldsymbol{r}(\tilde{\eta})) d\tilde{\eta}, \tag{36}$$

where

$$M(\eta, \tilde{\eta}) = \frac{\partial^2}{\partial\eta\partial\tilde{\eta}} \left\{ \frac{i}{2} H_0^{(1)}(\gamma_1 |\boldsymbol{r}(\eta) - \boldsymbol{r}(\tilde{\eta})|) + \frac{1}{2\pi} \log \left( 4 \sin^2 \frac{\eta - \tilde{\eta}}{2} \right) \right\}. \tag{37}$$

The kernel $M$ involves a weak singularity and it can be splitted as

$$M(\eta, \tilde{\eta}) = M_1(\eta, \tilde{\eta}) \log \left( 4 \sin^2 \frac{\eta - \tilde{\eta}}{2} \right) + M_2(\eta, \tilde{\eta}), \tag{38}$$

where

$$M_1(\eta, \tilde{\eta}) = -\frac{1}{2\pi} \frac{\partial^2}{\partial\eta\partial\tilde{\eta}} J_0(\gamma_1 |\boldsymbol{r}(\eta) - \boldsymbol{r}(\tilde{\eta})|), \tag{39}$$

and $M_2(\eta, \tilde{\eta})$ is evaluated through (38) except when $\eta = \tilde{\eta}$. In that case, we have

$$M_1(\eta, \eta) = -\frac{\gamma_1^2 |\boldsymbol{r}'(\eta)|^2}{4\pi}, \tag{40}$$

$$M_2(\eta, \eta) = \left( \pi i - 1 - 2C - 2 \log \frac{\gamma_1 |\boldsymbol{r}'(\eta)|}{2} \right) \frac{\gamma_1^2 |\boldsymbol{r}'(\eta)|^2}{4\pi} + \tag{41}$$

$$\frac{1}{12\pi} + \frac{[\boldsymbol{r}'(\eta) \cdot \boldsymbol{r}''(\eta)]^2}{2\pi |\boldsymbol{r}'(\eta)|^4} - \frac{|\boldsymbol{r}''(\eta)|^2}{4\pi |\boldsymbol{r}'(\eta)|^2} - \frac{\boldsymbol{r}'(\eta) \cdot \boldsymbol{r}'''(\eta)}{6\pi |\boldsymbol{r}'(\eta)|^2},$$

where $C = 0.57721 \cdots$ is Euler's constant. The first term in (36) can be approximated by the following quadrature formula:

$$\frac{1}{2\pi} \int_0^{2\pi} \cot \frac{\tilde{\eta} - \eta}{2} \phi'(\tilde{\eta}) d\tilde{\eta} \approx \sum_{l=0}^{N-1} T_l^N(\eta) \phi(\eta_l), \tag{42}$$

11

where

$$T_l^N(\eta) = -\frac{1}{N} \sum_{k=1}^{N/2-1} 2k \cos k(\eta - \eta_l) - \frac{1}{2} \cos \frac{N}{2}(\eta - \eta_l).$$

Using the trapezoidal rule and formulae (33) and (42), we obtain

$$|\boldsymbol{r}'(\eta)|(\mathcal{S}_1'\partial_\tau u)(\boldsymbol{r}(\eta)) \tag{43}$$
$$\approx \sum_{l=0}^{N-1} \left[ T_l^N(\eta) + M_1(\eta, \eta_l) R_l^N(\eta) + M_2(\eta, \eta_l) \right] u(\boldsymbol{r}(\eta_l)),$$

Therefore, the scaled hypersingular operator $|\boldsymbol{r}'|\mathcal{T}_1$ can be approximated. More details can be found in [34].

In the kernel-splitting procedure, Bessel functions $J_m(\gamma_j d)$ for integer $m$ and $d = |\boldsymbol{r} - \tilde{\boldsymbol{r}}|$ appear. For guided modes in dielectric waveguides, the propagation constant $\beta$ is real and it satisfies $k_0 n_2 < \beta < k_0 n_1$, thus $\gamma_2$ is a pure imaginary number. Since the Bessel functions $J_m$ grow exponentially along the imaginary axis, the kernel-splitting procedure presented above suffers numerical instability. To overcome this difficulty, Wang *et al.* [36] proposed to replace $J_m$ by a bounded function which approximates $J_m$ near the origin. For waveguides with a metallic core, $\gamma_1$ is a general complex number, thus the kernel-splitting procedure also suffers numerical instability for integral operators related to the waveguide core. The method of Wang *et al.* [36] is only applicable when $\gamma_j$ is pure imaginary. We extend their method to the case where $\gamma_j$ is a general complex number.

For a positive integer $M_*$, the Taylor expansion of $\exp(|\gamma_1 d|)J_m(\gamma_1 d)$ gives

$$e^{|\gamma_1 d|}J_m(\gamma_1 d) = \left(\frac{\gamma_1 d}{2}\right)^m \sum_{l=0}^{M_*-m} c_l |\gamma_1 d|^l + \mathcal{O}(|\gamma_1 d|^{M_*+1}), \quad d \to 0^+, \tag{44}$$

where

$$c_l = \sum_{k=0}^{[l/2]} \frac{e^{(2\arg\gamma_1+\pi)ki}}{k! \cdot (k+m)! \cdot 2^{2m} \cdot (l-2k)!}. \tag{45}$$

Let $\tilde{J}_m$ be the function given by

$$\tilde{J}_m(\gamma_1 d) = e^{-|\gamma_1 d|}\left(\frac{\gamma_1 d}{2}\right)^m \sum_{l=0}^{M_*-m} c_l |\gamma_1 d|^l. \tag{46}$$

It is a good approximation to $J_m(\gamma_1 d)$ for small $d$ and decays to zero as $d \to +\infty$. More precisely, we have

$$J_m(\gamma_1 d) - \tilde{J}_m(\gamma_1 d) = \mathcal{O}(|\gamma_1 d|)^{M+1}, \quad d \to 0^+. \tag{47}$$

12

With the replacement of $J_m$ by $\tilde{J}_m$, the kernel-splitting technique is stable for metallic waveguides.

## 5. Kernel-splitting technique: piecewise smooth case

In this section, we consider the discretization of boundary integral operators when $\Gamma$ is piecewise smooth. Based on a graded mesh [35] and the kernel-splitting technique presented in the previous section, the weakly singular integral operators can be easily discretized. The case for the hypersingular integral operator $\mathcal{T}_j$ is more complicated. A direct combination of the graded mesh and the splitting technique of Kress [34] fails. We develop a new splitting technique for $\mathcal{T}_j$ that works well with the graded mesh. The method should be useful to other problems where the hypersingular integral operator appears. We also present discretization schemes for the two functions $\mathcal{K}_0 1$ and $\mathcal{S}'_0 1$ that appear in the BIEs.

Let $\Gamma$ be represented by

$$\boldsymbol{r}(s) = (x(s), y(s)), \quad 0 \leq s \leq L,$$

where $s$ is the arclength and $L$ is the total length of $\Gamma$. We assume the corner points are given by $\boldsymbol{r}^j = \boldsymbol{r}(s_j)$ for $0 \leq j \leq j_*$, where $0 = s_0 < s_1 < ... < s_{j_*} = L$, and $s_0 = 0$ and $s_{j_*} = L$ correspond to the same corner point. A graded mesh [35, 33] on $\Gamma$ can be constructed from a piecewise sigmoidal function $s = w(\eta)$ for $0 \leq \eta \leq 2\pi$. The function $w$ is given explicitly as

$$w(\eta) = \frac{s_{j+1} w_1^p + s_j w_2^p}{w_1^p + w_2^p} \quad \text{for} \quad \eta^{(j)} \leq \eta \leq \eta^{(j+1)}, \quad j = 0, 1, ..., j_* - 1,$$

where the integer $p$ is the mesh order, $\eta^{(j)}$ corresponds to a corner point, i.e., $s_j = w(\eta^{(j)})$, and

$$w_1 = \left(\frac{1}{2} - \frac{1}{p}\right)\xi^3 + \frac{\xi}{p} + \frac{1}{2}, \quad w_2 = 1 - w_1, \quad \xi = \frac{2\eta - (\eta^{(j)} + \eta^{(j+1)})}{\eta^{(j+1)} - \eta^{(j)}}.$$

Notice that the derivatives of $w$ up to order $p - 1$ vanish at the corners. The graded mesh is obtained by discretizing $\eta$ uniformly with an even number of points: $\{\eta_l = 2\pi l/N\}_{l=0}^{N-1}$ where $N$ is even. We assume these discretization points contain all corner points, that is, for each $j$ satisfying $0 \leq j \leq j_* - 1$, there is an integer $l_j$ such that $\eta^{(j)} = \eta_{l_j}$.

13

Using the function $s = w(\eta)$, we reparameterize $\Gamma$ as

$$\boldsymbol{r}(\eta) = (x(w(\eta)), y(w(\eta))), \quad 0 \leq \eta \leq 2\pi. \tag{48}$$

For simplcity, we denote $\boldsymbol{r}(s) = \boldsymbol{r}(w(\eta))$ by $\boldsymbol{r}(\eta)$. Using the kernel-splitting technique presented in the previous section, the integral operators $\mathcal{S}_1$, $\mathcal{K}_1$ and $|\boldsymbol{r}'|\mathcal{K}_1'$ can be discretized, where $\boldsymbol{r}'$ is the derivative of $\boldsymbol{r}$ with respect to $\eta$. Notice that $|\boldsymbol{r}'(\eta)|$ is zero when $\eta$ corresponds to a corner and it is positive otherwise. Meanwhile, $\mathcal{K}_1'$ is not defined at the corners, since the normal vector $\boldsymbol{\nu}$ is not defined. Nevertheless, $|\boldsymbol{r}'|\mathcal{K}_1'$ is well-defined even at corners since $|\boldsymbol{r}'|\boldsymbol{\nu}$ vanishes there.

For the hypersingular operator $\mathcal{T}_1$, we also need to consider the scaled operator $|\boldsymbol{r}'|\mathcal{T}_1$. However, the kernel-splitting technique of Kress [34] does not work, since the diagonal term of $M_2$ in (41) blows up as $\eta$ tends to any corner point. In the following, we present a new kernel-splitting technique for $|\boldsymbol{r}'|\mathcal{T}_1$. Due to Maue's identity (34), the discretization of $|\boldsymbol{r}'|\mathcal{T}_1$ is reduced to the discretization of $|\boldsymbol{r}'|\mathcal{S}_1'\partial_{\boldsymbol{\tau}}u$. Splitting out the singular term, we obtain

$$|\boldsymbol{r}'(\eta)|(\mathcal{S}_1'\partial_{\boldsymbol{\tau}}u)(\boldsymbol{r}(\eta)) = \int_0^{2\pi} \left[ \frac{1}{2\pi} \cot \frac{\tilde{\eta} - \eta}{2} - Q(\eta, \tilde{\eta}) \right] \frac{du(\boldsymbol{r}(\tilde{\eta}))}{d\tilde{\eta}} d\tilde{\eta}, \tag{49}$$

where

$$Q(\eta, \tilde{\eta}) = \frac{i\gamma_1[\boldsymbol{r}(\eta) - \boldsymbol{r}(\tilde{\eta})] \cdot \boldsymbol{r}'(\eta)}{2|\boldsymbol{r}(\eta) - \boldsymbol{r}(\tilde{\eta})|} H_1^{(1)}(\gamma_1|\boldsymbol{r}(\eta) - \boldsymbol{r}(\tilde{\eta})|) + \frac{1}{2\pi} \cot \frac{\tilde{\eta} - \eta}{2}.$$

The above splitting is different from (36), since no integration by parts is performed. We further split $Q$ into two parts to reveal the logarithmic singularity. That is

$$Q(\eta, \tilde{\eta}) = Q_1(\eta, \tilde{\eta}) \log \left( 4 \sin^2 \frac{\eta - \tilde{\eta}}{2} \right) + Q_2(\eta, \tilde{\eta}), \tag{50}$$

where
$$Q_1(\eta, \tilde{\eta}) = \frac{\gamma_1[\boldsymbol{r}(\eta) - \boldsymbol{r}(\tilde{\eta})] \cdot \boldsymbol{r}'(\eta)}{2\pi|\boldsymbol{r}(\eta) - \boldsymbol{r}(\tilde{\eta})|} J_1(\gamma_1|\boldsymbol{r}(\eta) - \boldsymbol{r}(\tilde{\eta})|).$$

If $\eta \neq \tilde{\eta}$, $Q_2(\eta, \tilde{\eta})$ can be evaluated by Eq. (50). When $\eta = \tilde{\eta}$, we have

$$Q_1(\eta, \eta) = 0, \quad Q_2(\eta, \eta) = \frac{\boldsymbol{r}'(\eta) \cdot \boldsymbol{r}''(\eta)}{2\pi|\boldsymbol{r}'(\eta)|^2}. \tag{51}$$

14

Notice the diagonal term of $Q_2$ also blows up as $\eta$ tends to any corner point, but since the function $u'(\boldsymbol{r}(\tilde{\eta}))$ vanishes at corners (where $u'$ denotes $du/d\eta$), the whole term $Q_2(\eta, \tilde{\eta})u'(\boldsymbol{r}(\tilde{\eta}))$ can still be regarded as a $2\pi$-periodic smooth function of $\tilde{\eta}$. Therefore, using the trapezoidal rule and the quadrature formulae (33) and (42), we obtain

$$|\boldsymbol{r}'(\eta)|(\mathcal{S}_1'\partial_{\boldsymbol{\tau}}u)(\boldsymbol{r}(\eta)) \approx \sum_{l=0}^{N-1} T_l^N(\eta)u(\boldsymbol{r}(\eta_l)) \qquad (52)$$

$$+ \left[ R_l^N(\eta)Q_1(\eta, \eta_l) + \frac{2\pi}{N}Q_2(\eta, \eta_l) \right] \frac{du}{d\eta}(\boldsymbol{r}(\eta_l)).$$

To express the left hand side of (52) in terms of $u(\boldsymbol{r}(\eta_l))$ only, we need a relation between $du/d\eta = |\boldsymbol{r}'|\partial_{\boldsymbol{\tau}}u$ and $u$, i.e., the scaled tangential operator. This will be discussed it the next section.

Our BIEs contain two extra terms $\mathcal{K}_0 1$ and $\mathcal{S}_0' 1$. The evaluation of $\mathcal{K}_0 1$ is straightforward and is given in [35]. For the second term, we split out a singular term and obtain

$$(\mathcal{S}_0'1)(\boldsymbol{r}(\eta)) = \int_0^{2\pi} \left[ \frac{1}{2\pi} \cot \frac{\tilde{\eta} - \eta}{2} - U(\eta, \tilde{\eta}) \right] d\tilde{\eta}, \qquad (53)$$

where

$$U(\eta, \tilde{\eta}) = \frac{(\boldsymbol{r}(\tilde{\eta}) - \boldsymbol{r}(\eta)) \cdot \boldsymbol{r}'(\tilde{\eta})}{\pi|\boldsymbol{r}(\eta) - \boldsymbol{r}(\tilde{\eta})|^2} + \frac{1}{2\pi} \cot \frac{\tilde{\eta} - \eta}{2}, \quad \eta \neq \tilde{\eta}, \qquad (54)$$

and

$$U(\eta, \eta) = \frac{\boldsymbol{r}'(\eta) \cdot \boldsymbol{r}''(\eta)}{2\pi|\boldsymbol{r}'(\eta)|^2}. \qquad (55)$$

Since

$$\int_0^{2\pi} \frac{1}{2\pi} \cot \frac{\tilde{\eta} - \eta}{2} d\tilde{\eta} = 0,$$

the trapezoidal rule gives us

$$(\mathcal{S}_0'1)(\boldsymbol{r}(\eta)) \approx -\frac{2\pi}{N} \sum_{l=0}^{N-1} U(\eta, \eta_l). \qquad (56)$$

We can see that $U(\eta, \eta)$ blows up as $\eta$ tends to a corner. Nevertheless, if Eq. (25) is multiplied by $|\boldsymbol{r}'|$, then the $\mathcal{S}_0'1$ term has a multiplier $du/d\eta$ which vanishes at corners.

In the above kernel-splitting procedure for $|\boldsymbol{r}'|\mathcal{T}_1$, Bessel functions $J_m$ should be replaced by $\tilde{J}_m$ if necessary, to avoid numerical instability.

15

## 6. Discretization of DtN and NtD operators

In section 3, we presented BIEs (21) and (25) for the bounded domain $\Omega_1$ when its boundary $\Gamma$ is piecewise smooth. In principle, they can be discretized and be used to calculate the NtD and DtN operators as in (23) and (27). In practice, due to the use of a graded mesh, we need to use scaled operators that replace the normal derivative of the field $\partial_{\nu} u$ by $\psi = |\boldsymbol{r}'|\partial_{\nu} u$, where $\boldsymbol{r}$ is given in (48) and the prime denotes derivative with respect to $\eta$. The scaled DtN operator $\tilde{\Lambda}_1$ and the scaled NtD operator $\tilde{\mathcal{N}}_1$ satisfy

$$\tilde{\Lambda}_1 u = \psi, \quad \tilde{\mathcal{N}}_1 \psi = u \quad \text{on} \quad \Gamma, \tag{57}$$

for any $u$ satisfying the Helmholtz equation (3) in $\Omega_1$.

The tangential derivative operator $\partial_{\tau}$ appears in all eigenvalue-problem formulations (6), (8) and (11), and it is also needed in the process for evaluating the hypersingular operator $\mathcal{T}_1$. We also consider the scaled tangential operator $|\boldsymbol{r}'|\partial_{\tau}$ which is is simply the derivative with respect to $\eta$, that is $d/d\eta = |\boldsymbol{r}'|\partial_{\tau}$. If $\Gamma$ is smooth, $\partial_{\tau}$ can be approximated by a matrix based on the discrete Fourier transform (see for example, [32]). If $\Gamma$ is piecewise smooth, we may still regard functions on $\Gamma$ as smooth $2\pi$-periodic functions of $\eta$, and approximate $|\boldsymbol{r}'|\partial_{\tau}$ by a matrix using the discrete Fourier transform [33]. When $\eta$ is discretized by $N$ points, this leads to a full $N \times N$ matrix. Here, we present a better approach that approximates $d/d\eta$ on each smooth piece of $\Gamma$ based on the discrete cosine transform. As a result, $d/d\eta$ is approximated by a block diagonal matrix.

For a function $u$ on $\Gamma$, we denote $u(\boldsymbol{r}(\eta))$ by $u(\eta)$ for simplicity. On the $j$th interval of $\eta$, i.e., $[\eta^{(j)}, \eta^{(j+1)}]$ for $0 \leq j \leq j_* - 1$, if $u(\eta)$ is given at $N_j = l_{j+1} - l_j + 1$ points $\{\eta_l = 2\pi l/N \text{ for } l_j \leq l \leq l_{j+1}\}$, then $u(\eta)$ can be approximated by a finite cosine series

$$u(\eta) \approx \sum_{k=0}^{N_j-1} \hat{u}_k \cos \frac{\pi k(\eta - \eta^{(j)})}{\eta^{(j+1)} - \eta^{(j)}}, \tag{58}$$

where the coefficients are calculated by the discrete cosine transform, i.e.,

$$\hat{u}_k = \frac{1}{N_j - 1} \left[ u(\eta^{(j)}) + 2 \sum_{l=l_j+1}^{l_{j+1}-1} u(\eta_l) \cos \frac{\pi k(\eta_l - \eta^{(j)})}{\eta^{(j+1)} - \zeta^{(j)}} + (-1)^k u(\eta^{(j+1)}) \right]. \tag{59}$$

We can evaluate $du/d\eta$ at these $N_j$ points by (58):

$$\frac{du}{d\eta}(\eta_l) \approx \sum_{k=0}^{N_j-1} \frac{-\pi k \hat{u}_k}{\eta^{(j+1)} - \eta^{(j)}} \sin \frac{\pi k (\eta_l - \eta^{(j)})}{\eta^{(j+1)} - \eta^{(j)}}, \quad l = l_j, ..., l_j + 1. \qquad (60)$$

The above gives rise to a differentiation matrix $\mathcal{D}_j$ satisfying

$$\frac{d\boldsymbol{u}_j}{d\eta} = \mathcal{D}_j \boldsymbol{u}_j, \qquad (61)$$

where $d\boldsymbol{u}_j/d\eta$ and $\boldsymbol{u}_j$ are column vectors of $u'(\eta_l)$ and $u(\eta_l)$, respectively, for $l_j \leq l \leq l_{j+1}$.

The BIE (21) related to the NtD operator $\mathcal{N}_1$ contains the term $\mathcal{S}_1 \partial_{\boldsymbol{\nu}} u$. When the line integral on $\Gamma$ is transformed to the integral for $\eta$ on $[0, 2\pi]$, we have $ds(\boldsymbol{r}) = |\boldsymbol{r}'| d\eta$. Therefore, we can define a scaled operator $\tilde{\mathcal{S}}_1$, such that

$$\mathcal{S}_1 \partial_{\boldsymbol{\nu}} u = \tilde{\mathcal{S}}_1 \psi,$$

where $\psi = |\boldsymbol{r}'| \partial_{\boldsymbol{\nu}} u$. Eqs. (21) and (23) become

$$(\mathcal{K}_1 - \mathcal{K}_0 1) u = \tilde{\mathcal{S}}_1 \psi, \qquad (62)$$
$$\tilde{\mathcal{N}}_1 = (\mathcal{K}_1 - \mathcal{K}_0 1)^{-1} \tilde{\mathcal{S}}_1. \qquad (63)$$

To find a matrix approximation for the scaled NtD operator $\tilde{\mathcal{N}}_1$, we collocate $\eta$ at $\eta_l$ for $0 \leq l \leq N - 1$, apply the kernel-splitting techniques given in sections 5 and 6, and solve the linear system.

If we multiply BIE (25) by $|\boldsymbol{r}'|$ and define a scaled operator $\tilde{\mathcal{K}}'_1$ such that

$$|\boldsymbol{r}'| \mathcal{K}'_1 \partial_{\boldsymbol{\nu}} u = \tilde{\mathcal{K}}'_1 \psi,$$

then Eq. (25) is transformed to

$$(\tilde{\mathcal{K}}'_1 + \mathcal{K}_0 1) \psi = (\mathcal{S}'_0 1) |\boldsymbol{r}'| \partial_{\boldsymbol{\tau}} u + |\boldsymbol{r}'| \mathcal{T}_1 u. \qquad (64)$$

Therefore, we can calculate the scaled DtN operator $\tilde{\Lambda}_1$ by

$$\tilde{\Lambda}_1 = (\tilde{\mathcal{K}}'_1 + \mathcal{K}_0 1)^{-1} \left[ (\mathcal{S}'_0 1) \frac{d}{d\eta} + |\boldsymbol{r}'| \mathcal{T}_1 \right]. \qquad (65)$$

Based on the discretization schemes for $|\boldsymbol{r}'| \mathcal{K}'_1$ (easily revised for $\tilde{\mathcal{K}}'_1$), $|\boldsymbol{r}'| \mathcal{T}_1$, $\mathcal{K}_0 1$, $\mathcal{S}'_0 1$, $|\boldsymbol{r}'| \partial_{\boldsymbol{\tau}}$, and collocating $\eta$ at $\eta_l$ for $0 \leq l \leq N - 1$, we can then find a matrix approximating $\tilde{\Lambda}_1$.

In section 3, we claimed that consistent numerical evaluations of $\mathcal{K}_0 1$ and $\mathcal{S}'_0 1$ in the BIEs are useful for improving the accuracy. Here, we present a numerical example to support this claim. Let $\Omega_1 = \{(x, y) \mid 0 < x < 1\,\mu\text{m},\ 0 < y < 1\,\mu\text{m}\}$ be a square with refractive index $n_1 = 2$. Assuming $\beta = 4\,\mu\text{m}^{-1}$ and $k_0 = 2\pi/1.5\,\mu\text{m}^{-1}$, the Helmholtz equation (3) has the following analytic solution

$$u(\boldsymbol{r}) = H_0^{(1)}(\gamma_1|\boldsymbol{r} - \boldsymbol{r}_0|) \quad \text{in} \quad \Omega_1, \tag{66}$$

where $\boldsymbol{r}_0 = (-0.2, -0.2)\,\mu\text{m} \notin \Omega_1$ and $\gamma_1$ is defined in section 2. On the boundary $\Gamma$ (except at the corners), we have

$$\partial_{\boldsymbol{\nu}} u(\boldsymbol{r}) = -\frac{\gamma_1(\boldsymbol{r} - \boldsymbol{r}_0) \cdot \boldsymbol{\nu}(\boldsymbol{r})}{|\boldsymbol{r} - \boldsymbol{r}_0|} H_1^{(1)}(\gamma_1|\boldsymbol{r} - \boldsymbol{r}_0|). \tag{67}$$

We discretize $\Gamma$ by $N$ points using a graded mesh with a mesh order $p = 7$, and approximate the scaled DtN and NtD operators. The matrix approximations to these operators are denoted as $\tilde{\Lambda}_1^{(1)}$, $\tilde{\Lambda}_1^{(2)}$, $\tilde{\mathcal{N}}_1^{(1)}$ and $\tilde{\mathcal{N}}_1^{(2)}$, where the superscripts (1) and (2) correspond to discretizations without and with numerical evaluations of $\mathcal{K}_0 1$ and $\mathcal{S}'_0 1$. Let $\boldsymbol{u}$ and $\boldsymbol{\psi}$ be vectors of length $N$ corresponding to the exact values of $u$ and $\psi = |\boldsymbol{r}'|\partial_{\boldsymbol{\nu}} u$ at the $N$ points, we calculate the following errors

$$e_l^{\text{dtn}} = ||\boldsymbol{\psi} - \tilde{\Lambda}_1^{(l)}\boldsymbol{u}||_2, \quad e_l^{\text{ntd}} = ||\boldsymbol{u} - \tilde{\mathcal{N}}_1^{(l)}\boldsymbol{\psi}||_2, \quad l = 1, 2.$$

These errors are shown in Fig. 2 for different values of $N$. It is clear that the scaled DtN and NtD operators based on numerical evaluation of $\mathcal{K}_0 1$ and $\mathcal{S}'_0 1$ are more accurate. The top panel of Fig. 2 indicates a persistent large error for the NtD operator obtained without a numerical evaluation of $\mathcal{K}_0 1$. To see more details for this case, we show the pointwise absolute error for $N = 600$ in Fig. 3. It is clear that large errors occur around the four corners.

## 7. Revised formulation

When $\Gamma$ is piecewise smooth, the NtD, DtN and tangential derivative operators should all be replaced by their scaled versions to maintain numerical stability. As a result, the eigenvalue-problem formulations presented in section 2 must be revised accordingly.
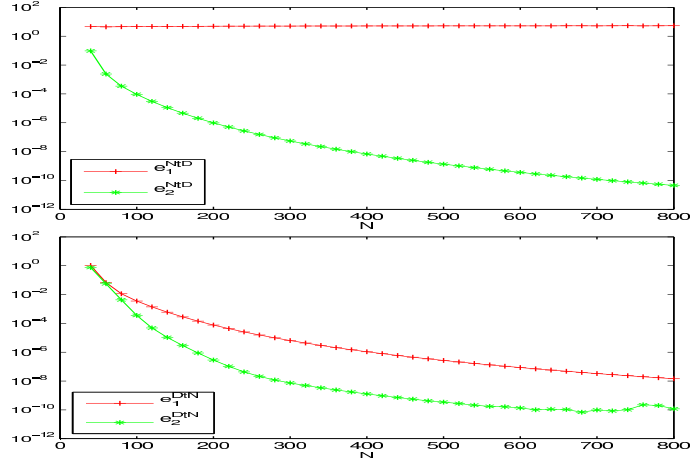
Figure 2: Comparing the scaled NtD and DtN operators obtained with ($l = 2$) and without ($l = 1$) numerical evaluations of $\mathcal{K}_0 1$ and $\mathcal{S}'_0 1$. Top: absolute errors $e_l^{\mathrm{ntd}}$ for $\tilde{\mathcal{N}}$ and $l = 1, 2$; Bottem: absolute errors $e_l^{\mathrm{dtn}}$ for $\tilde{\Lambda}$ and $l = 1, 2$.
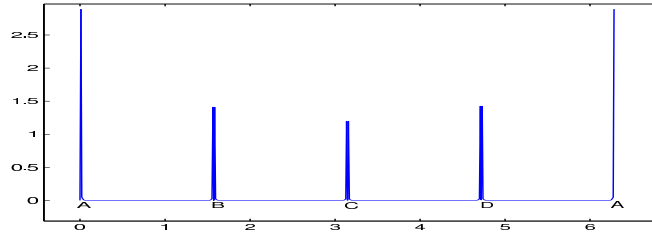


Figure 3: Absolute error $|u - \tilde{\mathcal{N}}_1^{(1)} \psi|$ of the scaled NtD operator without numerical evaluation of $\mathcal{K}_0 1$ vs. $\eta$ for $N = 600$.

19

The continuity of the terms in (5) implies the continuity of

$$\nu_x \psi_x + \nu_y \psi_y \quad \text{and} \quad \frac{1}{\varepsilon}\left[ (\nu_x \psi_y - \nu_y \psi_x) - \left( \nu_y \frac{dH_y}{d\eta} + \nu_x \frac{dH_x}{d\eta} \right) \right], \qquad (68)$$

where $\psi_x = |\boldsymbol{r}'|\partial_{\boldsymbol{\nu}} H_x$ and $\psi_y = |\boldsymbol{r}'|\partial_{\boldsymbol{\nu}} H_y$. Based on the above and multiplying both sides of Eq. (6) by $|\boldsymbol{r}'|$, we have

$$\left[ \begin{array}{cc} \nu_x \tilde{\Lambda}_2 - \nu_x \tilde{\Lambda}_1 & \nu_y \tilde{\Lambda}_2 - \nu_y \tilde{\Lambda}_1 \\ \rho\nu_x \frac{d}{d\eta} + \nu_y \tilde{\Pi} & \rho\nu_y \frac{d}{d\eta} - \nu_x \tilde{\Pi} \end{array} \right] \left[ \begin{array}{c} H_x \\ H_y \end{array} \right] = 0 \quad \text{on} \quad \Gamma, \qquad (69)$$

where $\tilde{\Pi} = \varepsilon_1^{-1}\tilde{\Lambda}_1 - \varepsilon_2^{-1}\tilde{\Lambda}_2$. Similarly, multiplying the first row of Eq. (11) by $|\boldsymbol{r}'|$ and replacing $\mathcal{N}_j$ by $\tilde{\mathcal{N}}_j(|\boldsymbol{r}'|\cdot)$, we have

$$\left[ \begin{array}{ccc} \varepsilon_1^{-1}\tilde{\mathcal{F}}_1 - \varepsilon_2^{-1}\tilde{\mathcal{F}}_2 & \varepsilon_2^{-1}\tilde{\mathcal{E}}_2 & -\varepsilon_1^{-1}\tilde{\mathcal{E}}_1 \\ (\tilde{\mathcal{N}}_2 - \tilde{\mathcal{N}}_1)(\nu_x\cdot) & -\tilde{\mathcal{N}}_2(\nu_y\cdot) & \tilde{\mathcal{N}}_1(\nu_y\cdot) \\ (\tilde{\mathcal{N}}_2 - \tilde{\mathcal{N}}_1)(\nu_y\cdot) & \tilde{\mathcal{N}}_2(\nu_x\cdot) & -\tilde{\mathcal{N}}_1(\nu_x\cdot) \end{array} \right] \left[ \begin{array}{c} \tilde{f} \\ \tilde{g}^+ \\ \tilde{g}^- \end{array} \right] = 0, \quad \text{on} \quad \Gamma, \qquad (70)$$

where $\tilde{f} = |\boldsymbol{r}'|f$, $\tilde{g}^{\pm} = |\boldsymbol{r}'|g^{\pm}$, $\tilde{\mathcal{E}}_j$ and $\tilde{\mathcal{F}}_j$ are defined by

$$\tilde{\mathcal{E}}_j = \tilde{\mathcal{A}}_j(\nu_x\cdot) + \tilde{\mathcal{B}}_j(\nu_y\cdot), \quad \tilde{\mathcal{F}}_j = -\tilde{\mathcal{A}}_j(\nu_y\cdot) + \tilde{\mathcal{B}}_j(\nu_x\cdot), \qquad (71)$$

and

$$\tilde{\mathcal{A}}_j = \nu_x - \nu_y \frac{d}{d\eta} \circ \tilde{\mathcal{N}}_j, \quad \tilde{\mathcal{B}}_j = \nu_y + \nu_x \frac{d}{d\eta} \circ \tilde{\mathcal{N}}_j. \qquad (72)$$

When $\Gamma$ is discretized by $N$ points, $d/d\eta$, $\tilde{\Lambda}_j$ and $\tilde{\mathcal{N}}_j$ are all approximated by $N \times N$ matrices, $\nu_x$ and $\nu_y$ are represented by $N \times N$ diagonal matrices. Therefore, the matrix operators in Eq. (69) and Eq. (70) are approximated by $(2N) \times (2N)$ and $(3N) \times (3N)$ matrices, respectively.

To find the propagation constant $\beta$, we follow a procedure proposed by Cheng *et al.* [30]. If the matrix approximations to (69) and (70) are denoted as

$$F(\beta)\boldsymbol{\phi} = 0, \qquad (73)$$

then we solve $\beta$ iteratively from the nonlinear equation

$$f(\beta) = \frac{1}{\boldsymbol{a}^T F^{-1}(\beta)\boldsymbol{b}} = 0, \qquad (74)$$

where $\boldsymbol{a}$ and $\boldsymbol{b}$ are two fixed random vectors. In each iteration, we solve the linear system $F(\beta)\boldsymbol{w} = \boldsymbol{b}$ to obtain $\boldsymbol{w} = F^{-1}(\beta)\boldsymbol{b}$.

## 8. Extensions

So far, we have only considered waveguides with a single homogeneous core surrounded by a homogeneous medium. In this section, we extend our work to more general waveguide structures. The first extension is for waveguides like photonic crystal fibers [4, 32]. The cross-section of such a waveguide consists of several homogeneous non-overlapping bounded domains (with possibly different refractive indices) surrounded by a homogeneous medium. To find guided modes for this kind of waveguides, we need to compute the scaled tangential derivative operator along each interface, find the scaled DtN and NtD operators for each bounded homogeneous domain and for the unbounded domain. Based on these operators and the continuity conditions along the interfaces, we can establish nonlinear eigenvalue problems like Eq. (69) and Eq. (70) with two or three functions on each interface. The final step for solving the propagation constant $\beta$ is the same as before.

The other extension is concerned with waveguides with a layered background medium. A typical example is the rib waveguide shown in Fig. 4. The
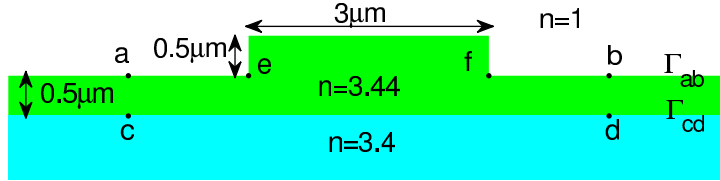


Figure 4: A rib waveguide involving a high index ($n = 3.44$) layer on a slightly lower index ($n = 3.4$) substrate with air cladding ($n = 1$). The thickness of the layer is $0.5\,\mu$m. The waveguide core is created by increasing the thickness of the high index layer to $1\,\mu$m for a width of $3\,\mu$m.

background is a thin high-index layer sandwiched between two lower-index media. The waveguide core is created by locally increasing the thickness of the high-index layer. The structure has three unbounded homogeneous domains corresponding to the three different refractive indices. The interfaces between these three domains extend to infinity. As before, the key step is to calculate the scaled tangential derivative operator for the interfaces and the scaled NtD and DtN operators for the homogeneous domains. Since the interfaces (the boundaries of the homogeneous domains) are unbounded, they must be truncated and the truncation leads to some errors. Fortunately, the wave field of a guided mode decays exponentially away from the waveguide

core, thus the boundary integral equations on truncated boundaries could still give accurate results.

To illustrate the basic ideas, we take the upper unbounded domain as an example. Let $\boldsymbol{a}$ and $\boldsymbol{b}$ be two points on the top interface sufficiently far away from the waveguide core such that $u$ and $\partial_\nu u$ are extremely close to zero on $B_{\boldsymbol{ab}}$, where $B_{\boldsymbol{ab}}$ is the top half circle with a diameter $\boldsymbol{ab}$ as shown in Fig. 4. Let $\Omega_1$ be the domain enclosed by $B_{\boldsymbol{ab}}$ and the curve $\Gamma_{\boldsymbol{ab}}$, and $\Gamma = B_{\boldsymbol{ab}} \cup \Gamma_{\boldsymbol{ab}}$ be the boundary of $\Omega_1$. As in section 3, we can establish two basic BIEs on $\Gamma$ corresponding to the DtN or NtD operators. If we further approximate $u$ and $\partial_\nu u$ on $B_{\boldsymbol{ab}}$ by zero, these two BIEs become

$$
2\!\!\!\!\!\fint_{\Gamma_{\boldsymbol{ab}}} \frac{\partial G^{(1)}(\boldsymbol{r},\tilde{\boldsymbol{r}})}{\partial \boldsymbol{\nu}(\tilde{\boldsymbol{r}})} u(\tilde{\boldsymbol{r}}) ds(\tilde{\boldsymbol{r}}) - 2\!\!\!\!\!\fint_{\Gamma} \frac{\partial G_0(\boldsymbol{r},\tilde{\boldsymbol{r}})}{\partial \boldsymbol{\nu}(\tilde{\boldsymbol{r}})} ds(\tilde{\boldsymbol{r}}) u(\boldsymbol{r})
$$
$$
\approx \; 2\int_{\Gamma_{\boldsymbol{ab}}} G^{(1)}(\boldsymbol{r},\tilde{\boldsymbol{r}}) \partial_\nu u(\tilde{\boldsymbol{r}}) ds(\tilde{\boldsymbol{r}}), \tag{75}
$$

$$
2\!\!\!\!\!\fint_{\Gamma_{\boldsymbol{ab}}} \frac{\partial G^{(1)}(\boldsymbol{r},\tilde{\boldsymbol{r}})}{\partial \boldsymbol{\nu}(\boldsymbol{r})} \partial_\nu u(\tilde{\boldsymbol{r}}) ds(\tilde{\boldsymbol{r}}) + 2\!\!\!\!\!\fint_{\Gamma} \frac{\partial G_0(\boldsymbol{r},\tilde{\boldsymbol{r}})}{\partial \boldsymbol{\nu}(\tilde{\boldsymbol{r}})} ds(\tilde{\boldsymbol{r}}) \partial_\nu u(\boldsymbol{r})
$$
$$
\approx \; 2\!\!\!\!\!\fint_{\Gamma} \frac{\partial G_0(\boldsymbol{r},\tilde{\boldsymbol{r}})}{\partial \boldsymbol{\tau}(\tilde{\boldsymbol{r}})} ds(\tilde{\boldsymbol{r}}) \partial_\tau u(\boldsymbol{r}) + 2\!\!\!\!\!\fint\!\!\!\!\!\fint_{\Gamma_{\boldsymbol{ab}}} \frac{\partial^2 G^{(1)}(\boldsymbol{r},\tilde{\boldsymbol{r}})}{\partial \boldsymbol{\nu}(\boldsymbol{r})\partial \boldsymbol{\nu}(\tilde{\boldsymbol{r}})} u(\tilde{\boldsymbol{r}}) ds(\tilde{\boldsymbol{r}}) \tag{76}
$$

for $\boldsymbol{r} \in \Gamma$, where $G^{(1)}$ is the Green's function for $\Omega_1$, and $\boldsymbol{r}$ in (76) must to be a smooth point of $\Gamma_{\boldsymbol{ab}}$. It is easy to show that

$$
2\!\!\!\!\!\fint_{B_{\boldsymbol{ab}}} \frac{\partial G_0(\boldsymbol{r},\tilde{\boldsymbol{r}})}{\partial \boldsymbol{\nu}(\tilde{\boldsymbol{r}})} ds(\tilde{\boldsymbol{r}}) \;=\; -\frac{\angle \boldsymbol{arb}}{\pi},
$$
$$
2\!\!\!\!\!\fint_{B_{\boldsymbol{ab}}} \frac{\partial G_0(\boldsymbol{r},\tilde{\boldsymbol{r}})}{\partial \boldsymbol{\tau}(\tilde{\boldsymbol{r}})} ds(\tilde{\boldsymbol{r}}) \;=\; -\frac{1}{\pi} \log \frac{|\boldsymbol{r}-\boldsymbol{a}|}{|\boldsymbol{r}-\boldsymbol{b}|}
$$

if $\boldsymbol{r}$ is neither $\boldsymbol{a}$ nor $\boldsymbol{b}$. Otherwise, we have

$$
2\!\!\!\!\!\fint_{\Gamma} \frac{\partial G_0(\boldsymbol{r},\tilde{\boldsymbol{r}})}{\partial \boldsymbol{\nu}(\tilde{\boldsymbol{r}})} ds(\tilde{\boldsymbol{r}}) = -1, \quad 2\!\!\!\!\!\fint_{\Gamma} \frac{\partial G_0(\boldsymbol{r},\tilde{\boldsymbol{r}})}{\partial \boldsymbol{\tau}(\tilde{\boldsymbol{r}})} ds(\tilde{\boldsymbol{r}}) = 0.
$$

Therefore, Eqs. (75) and (76) become

$$
2\!\!\!\!\!\fint_{\Gamma_{\boldsymbol{ab}}} \frac{\partial G^{(1)}(\boldsymbol{r},\tilde{\boldsymbol{r}})}{\partial \boldsymbol{\nu}(\tilde{\boldsymbol{r}})} u(\tilde{\boldsymbol{r}}) ds(\tilde{\boldsymbol{r}}) + \left( \frac{\angle \boldsymbol{arb}}{\pi} - 2\!\!\!\!\!\fint_{\Gamma_{\boldsymbol{ab}}} \frac{\partial G_0(\boldsymbol{r},\tilde{\boldsymbol{r}})}{\partial \boldsymbol{\nu}(\tilde{\boldsymbol{r}})} ds(\tilde{\boldsymbol{r}}) \right) u(\boldsymbol{r})
$$
$$
\approx 2\int_{\Gamma_{\boldsymbol{ab}}} G^{(1)}(\boldsymbol{r},\tilde{\boldsymbol{r}}) \partial_\nu u(\tilde{\boldsymbol{r}}) ds(\tilde{\boldsymbol{r}}), \tag{77}
$$

$$2 \fint_{\Gamma_{ab}} \frac{\partial G^{(1)}(\boldsymbol{r}, \tilde{\boldsymbol{r}})}{\partial \boldsymbol{\nu}(\boldsymbol{r})} \partial_{\nu} u(\tilde{\boldsymbol{r}}) ds(\tilde{\boldsymbol{r}}) - \left( \frac{\angle \boldsymbol{arb}}{\pi} - 2 \fint_{\Gamma_{ab}} \frac{\partial G_0(\boldsymbol{r}, \tilde{\boldsymbol{r}})}{\partial \boldsymbol{\nu}(\tilde{\boldsymbol{r}})} ds(\tilde{\boldsymbol{r}}) \right) \partial_{\nu} u(\boldsymbol{r})$$

$$\approx \left( 2 \fint_{\Gamma_{ab}} \frac{\partial G_0(\boldsymbol{r}, \tilde{\boldsymbol{r}})}{\partial \boldsymbol{\tau}(\tilde{\boldsymbol{r}})} ds(\tilde{\boldsymbol{r}}) - \frac{1}{\pi} \log \frac{|\boldsymbol{r} - \boldsymbol{a}|}{|\boldsymbol{r} - \boldsymbol{b}|} \right) \partial_{\tau} u(\boldsymbol{r})$$

$$+ 2 \fint_{\Gamma_{ab}} \frac{\partial^2 G^{(1)}(\boldsymbol{r}, \tilde{\boldsymbol{r}})}{\partial \boldsymbol{\nu}(\boldsymbol{r}) \partial \boldsymbol{\nu}(\tilde{\boldsymbol{r}})} u(\tilde{\boldsymbol{r}}) ds(\tilde{\boldsymbol{r}}). \tag{78}$$

By the definitions of integral operators (14)-(17), (22) and (26) (with $\Gamma$ replaced by $\Gamma_{ab}$), we can rewrite the above two BIEs as

$$\left( \frac{\angle \boldsymbol{arb}}{\pi} + \mathcal{K}_1 - \mathcal{K}_0 1 \right) u \approx \mathcal{S}_1 \partial_{\nu} u, \tag{79}$$

$$\left( \mathcal{K}_0 1 - \frac{\angle \boldsymbol{arb}}{\pi} + \mathcal{K}_1' \right) \partial_{\nu} u \approx \left( \mathcal{S}_0' 1 - \frac{1}{\pi} \log \frac{|\boldsymbol{r} - \boldsymbol{a}|}{|\boldsymbol{r} - \boldsymbol{b}|} \right) \partial_{\tau} u + \mathcal{T}_1 u. \tag{80}$$

Therefore, for the truncated domain $\Omega_1$, the NtD and NtD operators are given by

$$\mathcal{N}_1 \approx \left( \frac{\angle \boldsymbol{arb}}{\pi} + \mathcal{K}_1 - \mathcal{K}_0 1 \right)^{-1} \mathcal{S}_1, \tag{81}$$

$$\Lambda_1 \approx \left( \mathcal{K}_0 1 - \frac{\angle \boldsymbol{arb}}{\pi} + \mathcal{K}_1' \right)^{-1} \left[ \left( \mathcal{S}_0' 1 - \frac{1}{\pi} \ln \frac{|\boldsymbol{r} - \boldsymbol{a}|}{|\boldsymbol{r} - \boldsymbol{b}|} \right) \partial_{\tau} + \mathcal{T}_1 \right]. \tag{82}$$

The other two unbounded domains in Fig. 4 can be similarly handled. For actual numerical implementations, we need to use the revised operators.

Clearly, a large truncated boundary will give more accurate results, but it also requires more discretization points. Since the profile of a guided mode is smooth away from the waveguide core, it is desirable to use a larger mesh size near the end points of the truncated boundary. This can be achieved by a change of variable and using the new variable for discretization. For example, consider the line segment $\boldsymbol{fb}$ shown in Fig. 4 and assume that it is parameterized by its arclength $s$ for $0 \leq s \leq L$. We introduce a new variable $\tilde{s}$ for $0 \leq \tilde{s} \leq \tilde{L}$ (where $\tilde{L} < L$), such that $s = \tilde{s}$ for $0 \leq \tilde{s} \leq L_0 < L$ and

$$s = \tilde{s} + (L - \tilde{L}) \left( \frac{\tilde{s} - L_0}{\tilde{L} - L_0} \right)^{p+1}, \quad L_0 < \tilde{s} \leq \tilde{L},$$

where $p$ is the same integer used in the graded mesh for the corners. With this technique, we can calculate waveguide modes that decay slowly away from the core.

23

## 9. Numerical examples

In this section, we present several numerical examples. The first example is a right-angle trapezoidal dielectric waveguide as shown in Fig. 1(a). The height and the bottom base of the trapezoidal core are $12/23\,\mu$m and $1\,\mu$m, respectively, and the base angle is $48°$. The refractive indices of the waveguide core and the surrounding medium are $n_1 = \sqrt{8}$ and $n_2 = 1$, respectively. For this waveguide, we calculate its propagation constant $\beta$ for free space wavelength $\lambda = 1.5\,\mu$m by the original BIE-NtD method, the new BIE-NtD method and the BIE-DtN method. A reference solution $\beta_*/k_0 = 2.309472902955$ is obtained by extrapolating numerical solutions calculated by the original BIE-NtD method with graded mesh order $p = 7$, and it is used to calculate the absolute errors for numerical solutions corresponding to different values of $N$ (the number of discretization points on the interface $\Gamma$) and $p = 7$. The results for $160 \leq N \leq 800$ are shown in Fig. 5, where the vertical axis is the absolute error, the horizontal axis is $N_F$ or
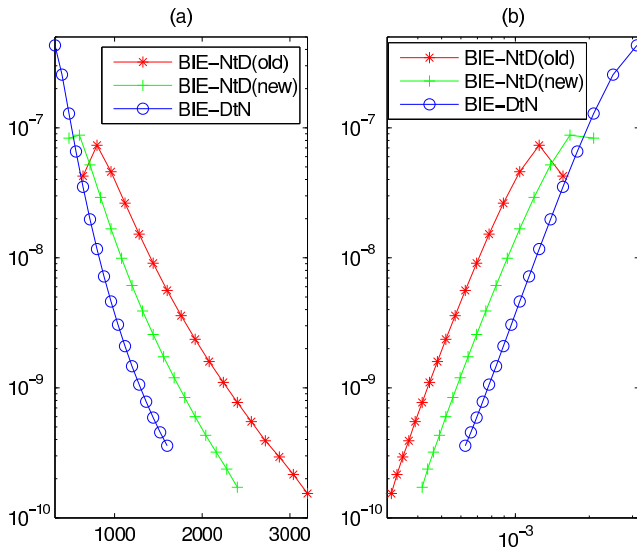


Figure 5: The trapezoidal dielectric waveguide: (a) the absolute error $|\beta - \beta_*|/k_0$ vs. $N_F$ for $p = 7$, where $\beta$ is the numerical solution; (b) the same absolute error vs. $1/N_F$.

$1/N_F$ in Fig. 5(a) or 5(b) respectively, $N_F$ is the size of the matrix $F$ in the final nonlinear eigenvalue problem (73). For the original BIE-NtD, the new BIE-NtD, and the BIE-DtN methods, $N_F = 4N$, $3N$ and $2N$, respectively. As expected, the three methods give about the same level of accuracy for the

same $N$, and the order of accuracy of these methods is about 5 as indicated by the slopes of the curves in Fig. 5(b), where both vertical and horizontal axes are shown in a logarithmic scale. Clearly, the BIE-DtN method has the lowest computation cost, but it is slightly less stable for large $N$. The new BIE-NtD method is useful when extremely high accuracy is needed.

The second example is the rectangular metallic waveguide shown in Fig. 1(b). It has a $0.15\,\mu\mathrm{m}\times0.3\,\mu\mathrm{m}$ metallic core with a refractive index $n_1 = 0.22+6.71i$ and the surrounding medium is air $(n_2 = 1)$. We calculate the propagation constant $\beta$ for free space wavelength $\lambda = 1\mu\mathrm{m}$, using $p = 7$ and for $160 \le N \le 800$. A reference solution $\beta_*/k_0 = 1.078814141 + 0.0039507129i$ is obtained by extrapolating numerical solutions computed by the new BIE-NtD method, and it is used to calculate the absolute errors for the less accurate numerical solutions. The absolute errors are shown in Fig. 6. As
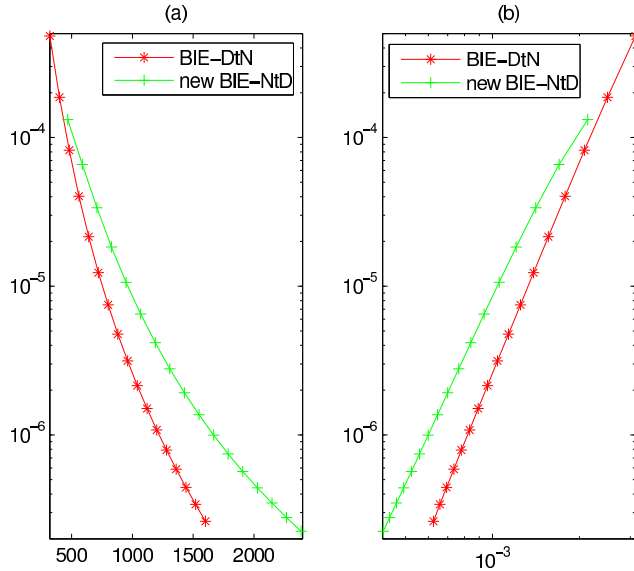


Figure 6: The rectangular metallic waveguide: (a) the absolute error $|\beta - \beta_*|/k_0$ vs. $N_F$ for $p = 7$, where $\beta$ is the numerical solution; (b) the same absolute error vs $1/N_F$.

before, these two methods exhibit about the same accuracy for the same $N$, the BIE-DtN method is more effcient, but the BIE-NtD method has better stability and is useful when high accuracy is needed. The orders of the methods depend on the field singularity at the corners. For this example, the order is about 4 as indicated by the slopes in Fig. 6(b).

The third example, as shown in Fig. 4, is a classical rib waveguide pre-

25

viously analyzed by a number of authors [10, 24]. The problem is difficult, since the eigenmode decays slowly in the horizontal direction. We calculate the propagation constant $\beta$ for $\lambda = 1.15\,\mu$m by the new BIE-NtD and BIE-DtN methods with graded mesh order $p = 6$. Numerical results using 160 discretization points on each smooth segment of the interfaces are shown in Table 1, and they are given for three different sizes of the truncated domain.

Table 1: The rib waveguide: numerical solutions $\beta/k_0$ for different truncated domains.

| Truncation | $\beta/k_0$(new BIE-NtD) | $\beta/k_0$(BIE-DtN) |
|---|---|---|
| $|x| < 7.5\mu$m | 3.41313213964 | 3.41313214393 |
| $|x| < 9.5\mu$m | 3.41313213964 | 3.41313214285 |
| $|x| < 11.5\mu$m | 3.41313213964 | 3.41313214021 |

For simplicity, we use the same number of points on each segment. Since there are six segments, the final matrix size is $N_F = 2880$ and $N_F = 1920$ for the BIE-NtD and BIE-DtN methods, respectively. Natually, the accuracy depends on the size of the truncated domain. It appears that both methods give the same solution $\beta/k_0 = 3.413132140$ after rounding. This is in good agreement with previous results of Hadley [10] ($\underline{3.413132} \pm 3 \times 10^{-6}$) and Chiang *et al.* [24] ($\underline{3.4131329}350$). These earlier results are calculated in truncated domains corresponding to $|x| < 3.8\,\mu$m and $|x| < 4.5\,\mu$m.

## 10. Conclusion

In the previous sections, we developed two new full-vectorial BIE methods for computing guided modes of optical waveguides. These methods are suitable for waveguides with a piecewise constant refractive index profile, where the interfaces are piecewise smooth and could have corners. High order full-vectorial mode solvers for waveguides with corners are difficult to develop due to the singularity of electromagnetic field at the corners. In each domain of constant refractive index, we derive BIEs with corner correction terms to calculate the NtD or DtN operators, and then formulate nonlinear eigenvalue problems for the propagation constant $\beta$ and some unknown functions defined on the interfaces. The new BIE-NtD and BIE-DtN methods solve three and two unknown functions, respectively. In contrast, the original BIE-NtD method [33] solves four functions, and the original BIE-DtN method [32] is only suitable for waveguides with smooth interfaces. The BIEs are discretized based on a Nyström method with kernel-splitting and graded

26

mesh techniques. In particular, a new kernel-splitting procedure is developed for the hypersingular boundary integral operator. Other improvements developed in this paper are concerned with the stability of the kernel-splitting technique for domains with complex refractive indices, the efficient evaluation of the tangential derivative operator, and the efficient truncation of unbounded interfaces. The new BIE-NtD and BIE-DtN method exhibit high order of accuracy, but the order depends on the graded mesh and the field singularity at the corners.

## Appendix

In this appendix, we give a derivation for Eqs. (21) and (25). For a bounded Lipschitz domain $\Omega_1$ with a piecewise smooth boundary $\Gamma$, we consider the following Neumann boundary value problem:

$$\begin{cases} \partial_x^2 u + \partial_y^2 u + \gamma_1^2 u = 0 & \text{in} \quad \Omega_1, \\ \frac{\partial u}{\partial \boldsymbol{\nu}} = g_N & \text{on } \Gamma, \end{cases} \tag{83}$$

where the Neumann data $g_N \in L^2(\Gamma)$. If $\gamma_1^2$ is not an eigenvalue of the negative Laplace operator on $\Omega_1$ with zero Neumann condition on $\Gamma$, then problem (83) admits a unique solution $u \in H^{3/2}(\Omega_1) \subset C^{0,1/2}(\bar{\Omega}_1)$ and $u|_\Gamma \in H^1(\Gamma) \subset C^{0,1/2}(\Gamma)$, indicating that

$$|u(\boldsymbol{r}) - u(\tilde{\boldsymbol{r}})| \le C_0 |\boldsymbol{r} - \tilde{\boldsymbol{r}}|^{\frac{1}{2}},$$

for any $\boldsymbol{r}, \tilde{\boldsymbol{r}} \in \bar{\Omega}_1$ where $C_0$ does not depend on these two points (see [38] and the references therein). Under the regularity conditions on $u$ and the domain $\Omega_1$, $u$ satisfies the following Green's representation theorem

$$u(\boldsymbol{r}) = \int_\Gamma \left[ G^{(1)}(\boldsymbol{r}, \tilde{\boldsymbol{r}}) \partial_{\boldsymbol{\nu}} u(\tilde{\boldsymbol{r}}) - \frac{\partial G^{(1)}(\boldsymbol{r}, \tilde{\boldsymbol{r}})}{\partial \boldsymbol{\nu}(\tilde{\boldsymbol{r}})} u(\tilde{\boldsymbol{r}}) \right] ds(\tilde{\boldsymbol{r}}), \quad \boldsymbol{r} \in \Omega_1. \tag{84}$$

Similarly, any harmonic function $u_0(\boldsymbol{r})$ satisfies

$$u_0(\boldsymbol{r}) = \int_\Gamma \left[ G_0(\boldsymbol{r}, \tilde{\boldsymbol{r}}) \partial_{\boldsymbol{\nu}} u_0(\tilde{\boldsymbol{r}}) - \frac{\partial G_0(\boldsymbol{r}, \tilde{\boldsymbol{r}})}{\partial \boldsymbol{\nu}(\tilde{\boldsymbol{r}})} u_0(\tilde{\boldsymbol{r}}) \right] ds(\tilde{\boldsymbol{r}}), \quad \boldsymbol{r} \in \Omega_1. \tag{85}$$

Let $u_0 = 1$, then Eq. (84) $- u(\boldsymbol{r}) \times$ Eq. (85) gives

$$\int_\Gamma \left[ \frac{\partial G^{(1)}(\boldsymbol{r}, \tilde{\boldsymbol{r}})}{\partial \boldsymbol{\nu}(\tilde{\boldsymbol{r}})} u(\tilde{\boldsymbol{r}}) - \frac{\partial G_0(\boldsymbol{r}, \tilde{\boldsymbol{r}})}{\partial \boldsymbol{\nu}(\tilde{\boldsymbol{r}})} u(\boldsymbol{r}) \right] ds(\tilde{\boldsymbol{r}}) = \int_\Gamma G^{(1)}(\boldsymbol{r}, \tilde{\boldsymbol{r}}) \partial_{\boldsymbol{\nu}} u(\tilde{\boldsymbol{r}}) ds(\tilde{\boldsymbol{r}}).$$
$$\tag{86}$$

To figure out what happens when $\boldsymbol{r}$ approaches the boundary $\Gamma$, we need the following lemma.

**Lemma 1.** *For a given function $f(\boldsymbol{r}, \tilde{\boldsymbol{r}}) \in C(\bar{\Omega}_1 \times \Gamma)$, if $\phi \in L^2(\Gamma)$, then*

$$\int_\Gamma \log |\boldsymbol{r} - \tilde{\boldsymbol{r}}| f(\boldsymbol{r}, \tilde{\boldsymbol{r}}) \phi(\tilde{\boldsymbol{r}}) ds(\boldsymbol{r}) \in C(\bar{\Omega}_1), \tag{87}$$

*and if $\phi \in L^\infty(\Gamma)$, then for any $\alpha_0 > 0$*

$$\int_\Gamma |\boldsymbol{r} - \tilde{\boldsymbol{r}}|^{\alpha_0 - 1} f(\boldsymbol{r}, \tilde{\boldsymbol{r}}) \phi(\tilde{\boldsymbol{r}}) ds(\boldsymbol{r}) \in C(\bar{\Omega}_1). \tag{88}$$

*Let $\boldsymbol{r}_*$ be given smooth point on $\Gamma$, $\Gamma_{\boldsymbol{r}_*}^d = B(\boldsymbol{r}_*, d) \cap \Gamma$ be a smooth part of $\Gamma$ for a proper $d > 0$, and $\Omega_{\boldsymbol{r}_*}^d = B(\boldsymbol{r}_*, d) \cap \Omega_1$. If $\phi \in L^2(\Gamma_{\boldsymbol{r}_*}^d)$, then*

$$\int_{\Gamma_{\boldsymbol{r}_*}^d} \log |\boldsymbol{r} - \tilde{\boldsymbol{r}}| f(\boldsymbol{r}, \tilde{\boldsymbol{r}}) \phi(\tilde{\boldsymbol{r}}) ds(\boldsymbol{r}) \in C(\overline{\Omega_{\boldsymbol{r}_*}^d}), \tag{89}$$

*and if $\phi \in L^\infty(\Gamma_{\boldsymbol{r}_*}^d)$, then for any $\alpha_0 > 0$*

$$\int_{\Gamma_{\boldsymbol{r}_*}^d} |\boldsymbol{r} - \tilde{\boldsymbol{r}}|^{\alpha_0 - 1} f(\boldsymbol{r}, \tilde{\boldsymbol{r}}) \phi(\tilde{\boldsymbol{r}}) ds(\boldsymbol{r}) \in C(\overline{\Omega_{\boldsymbol{r}_*}^d}). \tag{90}$$

For the proof of Lemma 1, see [40] and the references therein.

From the properties of Hankel functions, we can see that the nonregular part of $G^{(1)} - G_0$ is

$$\frac{1}{2\pi} \log(|\boldsymbol{r} - \tilde{\boldsymbol{r}}|)(1 - J_0(\gamma |\boldsymbol{r} - \tilde{\boldsymbol{r}}|)) = \mathcal{O}(|\boldsymbol{r} - \tilde{\boldsymbol{r}}|^2 \log |\boldsymbol{r} - \tilde{\boldsymbol{r}}|). \tag{91}$$

The integrand of the left hand side of Eq. (86) can be written as

$$\frac{\partial G^{(1)}(\boldsymbol{r}, \tilde{\boldsymbol{r}})}{\partial \boldsymbol{\nu}(\tilde{\boldsymbol{r}})} u(\tilde{\boldsymbol{r}}) - \frac{\partial G_0(\boldsymbol{r}, \tilde{\boldsymbol{r}})}{\partial \boldsymbol{\nu}(\tilde{\boldsymbol{r}})} u(\boldsymbol{r}) \tag{92}$$

$$= \frac{\partial (G^{(1)} - G_0)(\boldsymbol{r}, \tilde{\boldsymbol{r}})}{\partial \boldsymbol{\nu}(\tilde{\boldsymbol{r}})} u(\tilde{\boldsymbol{r}}) + \frac{\partial G_0(\boldsymbol{r}, \tilde{\boldsymbol{r}})}{\partial \boldsymbol{\nu}(\tilde{\boldsymbol{r}})} (u(\tilde{\boldsymbol{r}}) - u(\boldsymbol{r})),$$

$$= \sum_{i=1}^2 f_i(\boldsymbol{r}, \tilde{\boldsymbol{r}}) g_i(\tilde{\boldsymbol{r}}) + \sum_{i=3}^4 |\boldsymbol{r} - \tilde{\boldsymbol{r}}|^{-1/2} f_i(\boldsymbol{r}, \tilde{\boldsymbol{r}}) g_i(\tilde{\boldsymbol{r}}),$$

where $f_i \in C(\bar{\Omega}_1 \times \Gamma)$ and $g_i \in L^\infty(\Gamma)$ for $1 \leq i \leq 4$. For a given point $\boldsymbol{r}_* \in \Gamma$, as $\boldsymbol{r} \to \boldsymbol{r}_*$, by Lemma 1, Eq. (86) becomes

$$\int_\Gamma \left[ \frac{\partial G^{(1)}(\boldsymbol{r}_*, \tilde{\boldsymbol{r}})}{\partial \boldsymbol{\nu}(\tilde{\boldsymbol{r}})} u(\tilde{\boldsymbol{r}}) - \frac{\partial G_0(\boldsymbol{r}_*, \tilde{\boldsymbol{r}})}{\partial \boldsymbol{\nu}(\tilde{\boldsymbol{r}})} u(\boldsymbol{r}) \right] ds(\tilde{\boldsymbol{r}}) = \int_\Gamma G^{(1)}(\boldsymbol{r}_*, \tilde{\boldsymbol{r}}) \partial_\nu u(\tilde{\boldsymbol{r}}) ds(\tilde{\boldsymbol{r}}). \tag{93}$$

28

In light of this, Eq. (21) follows immediately from the fact that the improper integral $(\mathcal{K}_1 u)(\boldsymbol{r}_*)$ exists everywhere on $\Gamma$ since $u$ is Hölder continuous on $\Gamma$ (see [39]).

Next, we consider the Dirichlet boundary value problem

$$\begin{cases} \partial_x^2 u + \partial_y^2 u + \gamma_1^2 u = 0, & \text{in} \quad \Omega_1, \\ u = g_D, \quad \text{on } \Gamma, \end{cases} \tag{94}$$

where the Dirichlet data $g_D \in H^1(\Gamma)$. Again, if $\gamma_1^2$ is not an eigenvalue of the negative Laplace operator with zero Dirichlet boundary condition, then problem (94) admits a unique solution $u \in H^{3/2}(\Omega_1) \subset C^{0,1/2}(\bar{\Omega}_1)$ and $\partial_\nu u \in L^2(\Gamma)$ (see [38]). To establish Eq. (25), we require extra regularity conditions for $g_D$ on the smooth part of $\Gamma$.

Let $\boldsymbol{r}_*$ be a smooth point of $\Gamma$, using the notations in Lemma 1, we assume $g_D \in H^{\alpha_1+3/2}(\Gamma_{\boldsymbol{r}_*}^d)$ for any given positive $\alpha_1$. We conclude that $u \in H^{\alpha_1+2}(\Omega_{\boldsymbol{r}_*}^{d/2}) \subset C^{\alpha_1+1}(\overline{\Omega_{\boldsymbol{r}_*}^{d/2}})$ (see [38]). Let $\boldsymbol{r} = \boldsymbol{r}_* - \delta\boldsymbol{\nu}(\boldsymbol{r}_*)$ for $0 < \delta < d/2$ so that $\boldsymbol{r} \in \overline{\Omega_{\boldsymbol{r}_*}^{d/2}}$, and consider the directional derivative of Eqs. (84) and (85) in the direction $\boldsymbol{\nu}(\boldsymbol{r}_*)$. We have

$$\frac{\partial u(\boldsymbol{r})}{\partial \boldsymbol{\nu}(\boldsymbol{r}_*)} = \int_\Gamma \left[ \frac{\partial G^{(1)}(\boldsymbol{r},\tilde{\boldsymbol{r}})}{\partial \boldsymbol{\nu}(\boldsymbol{r}_*)} \partial_\nu u(\tilde{\boldsymbol{r}}) - \frac{\partial^2 G^{(1)}(\boldsymbol{r},\tilde{\boldsymbol{r}})}{\partial \boldsymbol{\nu}(\boldsymbol{r}_*)\partial \boldsymbol{\nu}(\tilde{\boldsymbol{r}})} u(\tilde{\boldsymbol{r}}) \right] ds(\tilde{\boldsymbol{r}}), \tag{95}$$

$$\frac{\partial u_0(\boldsymbol{r})}{\partial \boldsymbol{\nu}(\boldsymbol{r}_*)} = \int_\Gamma \left[ \frac{\partial G_0(\boldsymbol{r},\tilde{\boldsymbol{r}})}{\partial \boldsymbol{\nu}(\boldsymbol{r}_*)} \partial_\nu u_0(\tilde{\boldsymbol{r}}) - \frac{\partial^2 G_0(\boldsymbol{r},\tilde{\boldsymbol{r}})}{\partial \boldsymbol{\nu}(\boldsymbol{r}_*)\partial \boldsymbol{\nu}(\tilde{\boldsymbol{r}})} u_0(\tilde{\boldsymbol{r}}) \right] ds(\tilde{\boldsymbol{r}}). \tag{96}$$

Plugging $u_0 = x, y$ into Eq. (96), we obtain the following vectorial equation

$$\boldsymbol{\nu}(\boldsymbol{r}_*) = \int_\Gamma \left[ \frac{\partial G_0(\boldsymbol{r},\tilde{\boldsymbol{r}})}{\partial \boldsymbol{\nu}(\boldsymbol{r}_*)} \boldsymbol{\nu}(\tilde{\boldsymbol{r}}) - \frac{\partial^2 G_0(\boldsymbol{r},\tilde{\boldsymbol{r}})}{\partial \boldsymbol{\nu}(\boldsymbol{r}_*)\partial \boldsymbol{\nu}(\tilde{\boldsymbol{r}})} \tilde{\boldsymbol{r}} \right] ds(\tilde{\boldsymbol{r}}). \tag{97}$$

Considering Eq. (95)$-\nabla u(\boldsymbol{r})\cdot$ Eq. (97), we have

$$\left( \int_{\Gamma/\Gamma_{\boldsymbol{r}_*}^{d/2}} + \int_{\Gamma_{\boldsymbol{r}_*}^{d/2}} \right) \left[ \frac{\partial G^{(1)}(\boldsymbol{r},\tilde{\boldsymbol{r}})}{\partial \boldsymbol{\nu}(\boldsymbol{r}_*)} \partial_\nu u(\tilde{\boldsymbol{r}}) - \frac{\partial G_0(\boldsymbol{r},\tilde{\boldsymbol{r}})}{\partial \boldsymbol{\nu}(\boldsymbol{r}_*)} \nabla u(\boldsymbol{r}) \cdot \boldsymbol{\nu}(\tilde{\boldsymbol{r}}) \right] ds(\tilde{\boldsymbol{r}})$$

$$= \left( \int_{\Gamma/\Gamma_{\boldsymbol{r}_*}^{d/2}} + \int_{\Gamma_{\boldsymbol{r}_*}^{d/2}} \right) \left[ \frac{\partial^2 G^{(1)}(\boldsymbol{r},\tilde{\boldsymbol{r}})}{\partial \boldsymbol{\nu}(\boldsymbol{r}_*)\partial \boldsymbol{\nu}(\tilde{\boldsymbol{r}})} u(\tilde{\boldsymbol{r}}) - \frac{\partial^2 G_0(\boldsymbol{r},\tilde{\boldsymbol{r}})}{\partial \boldsymbol{\nu}(\boldsymbol{r}_*)\partial \boldsymbol{\nu}(\tilde{\boldsymbol{r}})} \nabla u(\boldsymbol{r}) \cdot \tilde{\boldsymbol{r}} \right] ds(\tilde{\boldsymbol{r}}). \tag{98}$$

Apparently, the integration of each side over $\Gamma/\Gamma_{\boldsymbol{r}_*}^{d/2}$ is continuous at $\boldsymbol{r} = \boldsymbol{r}_*$ as $\delta \to 0^+$. We now focus on the two integrations over the smooth part $\Gamma_{\boldsymbol{r}_*}^{d/2}$.

The integrand of the left hand side can be written as

$$\frac{\partial G^{(1)}(\boldsymbol{r}, \tilde{\boldsymbol{r}})}{\partial \boldsymbol{\nu}(\boldsymbol{r}_*)} \partial_{\boldsymbol{\nu}} u(\tilde{\boldsymbol{r}}) - \frac{\partial G_0(\boldsymbol{r}, \tilde{\boldsymbol{r}})}{\partial \boldsymbol{\nu}(\boldsymbol{r}_*)} \nabla u(\boldsymbol{r}) \cdot \boldsymbol{\nu}(\tilde{\boldsymbol{r}})$$

$$= \frac{\partial (G^{(1)} - G_0)(\boldsymbol{r}, \tilde{\boldsymbol{r}})}{\partial \boldsymbol{\nu}(\boldsymbol{r}_*)} \partial_{\boldsymbol{\nu}} u(\tilde{\boldsymbol{r}}) + \frac{\partial G_0(\boldsymbol{r}, \tilde{\boldsymbol{r}})}{\partial \boldsymbol{\nu}(\boldsymbol{r}_*)} (\nabla u(\tilde{\boldsymbol{r}}) - \nabla u(\boldsymbol{r})) \cdot \boldsymbol{\nu}(\tilde{\boldsymbol{r}}),$$

$$= \sum_{i=5}^{6} f_i(\boldsymbol{r}, \tilde{\boldsymbol{r}}) g_i(\tilde{\boldsymbol{r}}) + \sum_{i=7}^{10} f_i(\boldsymbol{r}, \tilde{\boldsymbol{r}}) g_i(\tilde{\boldsymbol{r}})$$

where $f_i \in C(\overline{\Omega_{\boldsymbol{r}_*}^{d/2}} \times \Gamma_{\boldsymbol{r}_*}^{d/2})$ for $5 \le i \le 10$, $g_i \in L^2(\Gamma_{\boldsymbol{r}_*}^{d/2})$ for $5 \le i \le 6$ and $g_i \in L^\infty(\Gamma_{\boldsymbol{r}_*}^{d/2})$ for $7 \le i \le 10$, and therefore it is continuous at $\boldsymbol{r} = \boldsymbol{r}_*$ as $\delta \to 0^+$ due to Lemma 1.

Taking $u_0 = 1$, Eq. (96) becomes

$$\int_\Gamma \frac{\partial^2 G_0(\boldsymbol{r}, \tilde{\boldsymbol{r}})}{\partial \boldsymbol{\nu}(\boldsymbol{r}_*) \partial \boldsymbol{\nu}(\tilde{\boldsymbol{r}})} ds(\tilde{\boldsymbol{r}}) = 0. \tag{99}$$

Therefore, the integral in the right hand side of Eq. (98) equals to

$$\int_\Gamma \left\{ \frac{\partial^2 (G^{(1)} - G_0)(\boldsymbol{r}, \tilde{\boldsymbol{r}})}{\partial \boldsymbol{\nu}(\boldsymbol{r}_*) \partial \boldsymbol{\nu}(\tilde{\boldsymbol{r}})} u(\tilde{\boldsymbol{r}}) + \frac{\partial^2 G_0(\boldsymbol{r}, \tilde{\boldsymbol{r}})}{\partial \boldsymbol{\nu}(\boldsymbol{r}_*) \partial \boldsymbol{\nu}(\tilde{\boldsymbol{r}})} [u(\tilde{\boldsymbol{r}}) - u(\boldsymbol{r}) - \nabla u(\boldsymbol{r}) \cdot (\tilde{\boldsymbol{r}} - \boldsymbol{r})] \right\} ds(\tilde{\boldsymbol{r}}).$$

Its integrand can be written as

$$\sum_{i=11}^{14} \log |\boldsymbol{r} - \tilde{\boldsymbol{r}}| f_i(\boldsymbol{r}, \tilde{\boldsymbol{r}}) g_i(\tilde{\boldsymbol{r}}) + \sum_{i=15}^{19} |\boldsymbol{r} - \tilde{\boldsymbol{r}}|^{\alpha_1/2 - 1} f_i(\boldsymbol{r}, \tilde{\boldsymbol{r}}) g_i(\tilde{\boldsymbol{r}}), \tag{100}$$

where $f_i \in C(\overline{\Omega_{\boldsymbol{r}_*}^{d/2}} \times \Gamma_{\boldsymbol{r}_*}^{d/2})$ and $g_i \in L^\infty(\Gamma_{\boldsymbol{r}_*}^{d/2})$ for $11 \le i \le 19$. Integrated over $\Gamma_{\boldsymbol{r}_*}^{d/2}$, the integration is continuous at $\boldsymbol{r} = \boldsymbol{r}_*$ as $\delta \to 0^+$ due to Lemma 1.

Therefore, taking the limit $\delta \to 0^+$ in Eq. (98), we have

$$\int_\Gamma \left[ \frac{\partial G^{(1)}(\boldsymbol{r}_*, \tilde{\boldsymbol{r}})}{\partial \boldsymbol{\nu}(\boldsymbol{r}_*)} \partial_{\boldsymbol{\nu}} u(\tilde{\boldsymbol{r}}) - \frac{\partial G_0(\boldsymbol{r}_*, \tilde{\boldsymbol{r}})}{\partial \boldsymbol{\nu}(\boldsymbol{r}_*)} \nabla u(\boldsymbol{r}_*) \cdot \boldsymbol{\nu}(\tilde{\boldsymbol{r}}) \right] ds(\tilde{\boldsymbol{r}})$$

$$= \int_\Gamma \left\{ \frac{\partial^2 G^{(1)}(\boldsymbol{r}_*, \tilde{\boldsymbol{r}})}{\partial \boldsymbol{\nu}(\boldsymbol{r}_*) \partial \boldsymbol{\nu}(\tilde{\boldsymbol{r}})} u(\tilde{\boldsymbol{r}}) + \frac{\partial^2 G_0(\boldsymbol{r}_*, \tilde{\boldsymbol{r}})}{\partial \boldsymbol{\nu}(\boldsymbol{r}_*) \partial \boldsymbol{\nu}(\tilde{\boldsymbol{r}})} [-u(\boldsymbol{r}_*) - \nabla u(\boldsymbol{r}_*) \cdot (\tilde{\boldsymbol{r}} - \boldsymbol{r}_*)] \right\} ds(\tilde{\boldsymbol{r}}) \tag{101}$$

To simplify this equation, we make use of the following two identities

$$\oint_\Gamma \frac{\partial^2 G_0(\boldsymbol{r}_*,\tilde{\boldsymbol{r}})}{\partial\boldsymbol{\nu}(\boldsymbol{r}_*)\partial\boldsymbol{\nu}(\tilde{\boldsymbol{r}})}ds(\tilde{\boldsymbol{r}}) = 0,$$

$$\oint_\Gamma \frac{\partial^2 G_0(\boldsymbol{r}_*,\tilde{\boldsymbol{r}})}{\partial\boldsymbol{\nu}(\boldsymbol{r}_*)\partial\boldsymbol{\nu}(\tilde{\boldsymbol{r}})}\tilde{\boldsymbol{r}}ds(\tilde{\boldsymbol{r}}) = \oint_\Gamma \frac{\partial G_0(\boldsymbol{r}_*,\tilde{\boldsymbol{r}})}{\partial\boldsymbol{\tau}(\boldsymbol{r}_*)}\boldsymbol{\tau}(\tilde{\boldsymbol{r}})ds(\tilde{\boldsymbol{r}}).$$

These two identities can be proved based on the fact that

$$\frac{\partial^2 G_0(\boldsymbol{r}_*,\tilde{\boldsymbol{r}})}{\partial\boldsymbol{\nu}(\boldsymbol{r}_*)\partial\boldsymbol{\nu}(\tilde{\boldsymbol{r}})} = -\frac{\partial^2 G_0(\boldsymbol{r}_*,\tilde{\boldsymbol{r}})}{\partial\boldsymbol{\tau}(\boldsymbol{r}_*)\partial\boldsymbol{\tau}(\tilde{\boldsymbol{r}})}, \quad \text{if} \quad \boldsymbol{r}_* \neq \tilde{\boldsymbol{r}}.$$

Observing $\nabla_{\boldsymbol{r}_*} G_0(\boldsymbol{r}_*,\tilde{\boldsymbol{r}}) = -\nabla_{\tilde{\boldsymbol{r}}} G_0(\boldsymbol{r}_*,\tilde{\boldsymbol{r}})$, we have

$$\oint_\Gamma \frac{\partial G_0(\boldsymbol{r}_*,\tilde{\boldsymbol{r}})}{\partial\boldsymbol{\nu}(\boldsymbol{r}_*)}\boldsymbol{\nu}(\tilde{\boldsymbol{r}})ds(\tilde{\boldsymbol{r}}) - \oint_\Gamma \frac{\partial^2 G_0(\boldsymbol{r}_*,\tilde{\boldsymbol{r}})}{\partial\boldsymbol{\nu}(\boldsymbol{r}_*)\partial\boldsymbol{\nu}(\tilde{\boldsymbol{r}})}\tilde{\boldsymbol{r}}ds(\tilde{\boldsymbol{r}})$$

$$= \oint_\Gamma \left[(\nabla_{\boldsymbol{r}_*} G_0(\boldsymbol{r}_*,\tilde{\boldsymbol{r}}) \cdot \boldsymbol{\nu}(\boldsymbol{r}_*))\boldsymbol{\nu}(\tilde{\boldsymbol{r}}) - (\nabla_{\boldsymbol{r}_*} G_0(\boldsymbol{r}_*,\tilde{\boldsymbol{r}}) \cdot \boldsymbol{\tau}(\boldsymbol{r}_*))\boldsymbol{\tau}(\tilde{\boldsymbol{r}})\right]ds(\tilde{\boldsymbol{r}})$$

$$= \oint_\Gamma [-\boldsymbol{\nu}(\tilde{\boldsymbol{r}})\boldsymbol{\nu}(\boldsymbol{r}_*)^T + \boldsymbol{\tau}(\tilde{\boldsymbol{r}})\boldsymbol{\tau}(\boldsymbol{r}_*)^T]\nabla_{\tilde{\boldsymbol{r}}} G_0(\boldsymbol{r}_*,\tilde{\boldsymbol{r}})ds(\tilde{\boldsymbol{r}})$$

$$= \oint_\Gamma [-\boldsymbol{\nu}(\tilde{\boldsymbol{r}})\boldsymbol{\nu}(\boldsymbol{r}_*)^T + \boldsymbol{\tau}(\tilde{\boldsymbol{r}})\boldsymbol{\tau}(\boldsymbol{r}_*)^T]^T\nabla_{\tilde{\boldsymbol{r}}} G_0(\boldsymbol{r}_*,\tilde{\boldsymbol{r}})ds(\tilde{\boldsymbol{r}})$$

$$= -\oint_\Gamma \frac{\partial G_0(\boldsymbol{r}_*,\tilde{\boldsymbol{r}})}{\partial\boldsymbol{\nu}(\tilde{\boldsymbol{r}})}ds(\tilde{\boldsymbol{r}})\boldsymbol{\nu}(\boldsymbol{r}_*) + \oint_\Gamma \frac{\partial G_0(\boldsymbol{r}_*,\tilde{\boldsymbol{r}})}{\partial\boldsymbol{\tau}(\tilde{\boldsymbol{r}})}ds(\tilde{\boldsymbol{r}})\boldsymbol{\tau}(\boldsymbol{r}_*).$$

Thus, Eq. (101) becomes

$$\oint_\Gamma \frac{\partial G_0(\boldsymbol{r}_*,\tilde{\boldsymbol{r}})}{\partial\boldsymbol{\nu}(\tilde{\boldsymbol{r}})}ds(\tilde{\boldsymbol{r}})\partial_\nu u(\boldsymbol{r}_*) + \oint_\Gamma \frac{\partial G(\boldsymbol{r}_*,\tilde{\boldsymbol{r}})}{\partial\boldsymbol{\nu}(\boldsymbol{r}_*)}\partial_\nu u(\tilde{\boldsymbol{r}})ds(\tilde{\boldsymbol{r}})$$

$$= \oint_\Gamma \frac{\partial G_0(\boldsymbol{r}_*,\tilde{\boldsymbol{r}})}{\partial\boldsymbol{\tau}(\tilde{\boldsymbol{r}})}ds(\tilde{\boldsymbol{r}})\partial_\tau u(\boldsymbol{r}_*) + \oint_\Gamma \frac{\partial^2 G(\boldsymbol{r}_*,\tilde{\boldsymbol{r}})}{\partial\boldsymbol{\nu}(\boldsymbol{r}_*)\partial\boldsymbol{\nu}(\tilde{\boldsymbol{r}})}u(\tilde{\boldsymbol{r}})ds(\tilde{\boldsymbol{r}}).$$

Notice that under the regularity conditions on $u$, all improper integrals above exist [39]. Therefore, at any smooth point of $\Gamma$, if we impose the same regularity condition on $g_D$ as argued before, then Eq. (25) is valid at all smooth points on $\Gamma$.

## References

[1] A. W. Snyder and J. D. Love, *Optical Waveguide Theory*, Chapman and Hall, London, 1983.

[2] D. Marcuse, *Theory of Dielectric Optical Waveguides*, 2nd ed., Academic Press, Boston, 1991.

[3] C. Vassallo, *Optical Waveguide Concepts*, Elsevier, Amsterdam, 1991.

[4] F. Poli, A. Cucinotta, and S. Selleri, *Photonic Crystal Fibers: Properties and Applications*, Springer, 2007.

[5] S. A. Maier, *Plasmonics: Fundamentals and Applications*, Springer, 2007.

[6] K. Bierwirth, N. Schulz, and F. Arndt, *Finite-difference analysis of rectangular dielectric wave-guide structures*, IEEE Trans. Microwave Theory Tech., 34 (1986), pp. 1104-1114.

[7] H. A. Jamid and M. N. Akram, *A new higher order finite-difference approximation scheme for the method of lines*, J. Lightwave Technol., 19 (2001), pp. 398-404.

[8] N. N. Feng, G. R. Zhou, C. L. Xu, and W. P. Huang, *Computation of full-vector modes for bending waveguide using cylindrical perfectly matched layers*, J. Lightwave Technol., 20 (2002), pp. 1976-1980.

[9] G. R. Hadley, *High-accuracy finite-difference equations for dielectric waveguide analysis I: Uniform regions and dielectric interfaces*, J. Lightwave Technol., 20 (2002), pp. 1210-1218.

[10] G. R. Hadley, *High-accuracy finite-difference equations for dielectric waveguide analysis II: Dielectric corners*, J. Lightwave Technol., 20 (2002), pp. 1219-1231.

[11] C. P. Yu and H. C. Chang, *Yee-mesh-based finite difference eigenmode solver with PML absorbing boundary conditions for optical waveguides and photonic crystal fibers*, Opt. Express, 12 (2004), pp. 6165-6177.

[12] M. Wik, D. Dumas, and D. Yevick, *Comparison of vector finite-difference techniques for modal analysis*, J. Opt. Soc. Am. A, 22 (2005), pp. 1341-1347.

[13] N. Thomas, P. Sewell, and T. M. Benson, *A new full-vectorial higher order finite-difference scheme for the modal analysis of rectangular dielectric waveguides*, J. Lightwave Technol., 25 (2007), pp. 2563-2570.

[14] Y. P. Chiou, Y. C. Chiang, C. H. Lai, C. H. Du, and H. C. Chang, *Finite difference modeling of dielectric waveguides with corners and slanted facets*, J. Lightwave Technol., 27 (2009), pp. 2077-2086.

[15] B. M. A. Rahman and J. B. Davies, *Finite-element solution of integrated optical wave-guides*, J. Lightwave Technol., 2 (1984), pp. 682-688.

[16] M. Koshiba, K. Hayata, and M. Suzuki, *Vectorial finite-element method without spurious solutions for dielectric waveguide problems*, Electronics Letters, 20 (1984), pp. 409-410.

[17] Z.-E. Abid, K. L. Johnson, and A. Gopinath, *Analysis of dielectric guides by vector tranverse magnetic field finite elements*, J. Lightwave Technol., 11 (1993), pp. 1545-1549.

[18] M. Koshiba, S. Maruyama, and K. Hirayama, *A vector finite-element method with the high-order mixed-interpolation-type triangular elements for optical wave-guiding problems*, J. Lightwave Technol., 12 (1994), pp. 495-502.

[19] M. Koshiba and Y. Tsuji, *Curvilinear hybrid edge/nodal elements with triangular shape for guided-wave problems*, J. Lightwave Technol., 18 (2000), pp. 737-743.

[20] S. Selleri, L. Vincetti L, A. Cucinotta, and M. Zoboli, *Complex FEM modal solver of optical waveguides with PML boundary conditions*, Opt. Quant. Electron., 33 (2001), pp. 359-371.

[21] S. S. A. Obayya, B. M. A. Rahman, K. T. V. Grattan, and H. A. El-Mikati, *Full vectorial finite-element-based imaginary distance beam propagation solution of complex modes in optical waveguides*, J. Lightwave Technol., 20 (2002), pp. 1054-1060.

[22] J. H. Yuan, *An adaptive inverse iteration FEM for the inhomogeneous dielectric waveguides*, Journal of Computational Mathematics, 25 (2007), pp. 169-184.

[23] C. C. Huang, C. C. Huang, and J. Y. Yang, *A full-vectorial pseudospectral modal analysis of dielectric optical waveguides with stepped refractive index profiles*, IEEE Journal of Selected Topics in Quantum Electronics, 11 (2005), pp. 457-465.

[24] P. J. Chiang, C. L. Wu, C. H. Teng, C. S. Yang, and H. C. Chang, *Full-vectorial optical waveguide mode solvers using multidomain pseudospectral frequency-domain (PSFD) formulations*, IEEE Journal of Quantum Electronics, 44 (2008) pp. 56-66.

[25] S. F. Chiang, B. Y. Lin, C. H. Teng, and H. C. Chang, *Improved analysis of rectangular dielectric waveguides based on a Legendre pseudospectral penalty scheme*, Integrated Photonics Research, Silicon and Nano Photonics on CDROM, paper IWH8, The Optical Society, Washington, DC, 2010.

[26] N. Guan, S. Habu, K. Takenaga, K. Himeno, and A. Wada, *Boundary Element Method for Analysis of Holey Optical Fibers*, jlt, 21 (2003), pp. 1787-1792.

[27] T. Lu and D. Yevick, *A vectorial boundary element method analysis of integrated optical waveguides*, J. Lightwave Technol., 21 (2003), pp. 1793-1807.

[28] T. Lu and D. Yevick, *Comparative evaluation of a novel series approximation for electromagnetic fields at dielectric corners with boundary element method applications*, J. Lightwave Technol., 22 (2004), pp. 1426-1432.

[29] S. V. Boriskina, T. M. Benson, P. Sewell, and A. I. Nosich, *Highly efficient full-vectorial integral equation solution for the bound, leaky and complex modes of dielectric waveguides*, IEEE J. Sel. Top. Quantum Electron., 8 (2002), pp. 1225-1231.

[30] H. Cheng, W. Y. Crutchfield, M. Doery, and L. Greengard, *Fast, accurate integral equation methods for the analysis of photonic crystal fibers I: Theory*, Opt. Express, 12(2004), pp. 3791-3805.

[31] E. Pone, A. Hassani, S. Lacroix, A. Kabashin, and M. Skorobogatiy, *Boundary integral method for the challenging problems in bandgap guiding, plasmonics and sensing*, Opt. Express, 15 (2007), pp. 10231-10246.

[32] W. Lu, Y. Y. Lu, *Efficient boundary integral equation method for photonic crystal fibers*, J. Lightwave Technol., 20 (2012), pp. 1610-1616.

[33] W. Lu, Y. Y. Lu, *Waveguide mode solver based on Neumann-to-Dirichlet operators and boundary integral equations*, J. Comput. Phys., 231 (2012), pp. 1360-1371.

[34] R. Kress, *On the numerical solution of a hypersingular integral equation in scattering theory*, J. Comput. Appl. Math., 61 (1995), pp. 345-360.

[35] D. Colton, R. Kress, *Inverse Acoustic and Electromagnetic Scattering Theory*, second ed., Springer-Verlag, Berlin, 1998.

[36] L. Wang, J. A. Cox, and A. Friedman, *Model analysis of homogeneous optical waveguides by the boundary integral formulation and the Nyström method*, J. Opt. Soc. Am. A, 15 (1998), pp. 92-100.

[37] E. Martensen, *Über eine methode zum räumlichen neumannschen problem mit einer anwendung für torusartige berandungen*, Acta Math., 109 (1963), pp. 75-135.

[38] W. McLean, *Strongly Elliptic Systems and Boundary Integral Equations*, Cambridge, University Press, Cambridge, 2000.

[39] R. Kress, *Linear integral equations*, Springer Verlag, 1999.

[40] F. Hartmann, "Elastic potentials on piecewise smooth surfaces", J. Elasticity, 12 (1982), pp. 31-50.